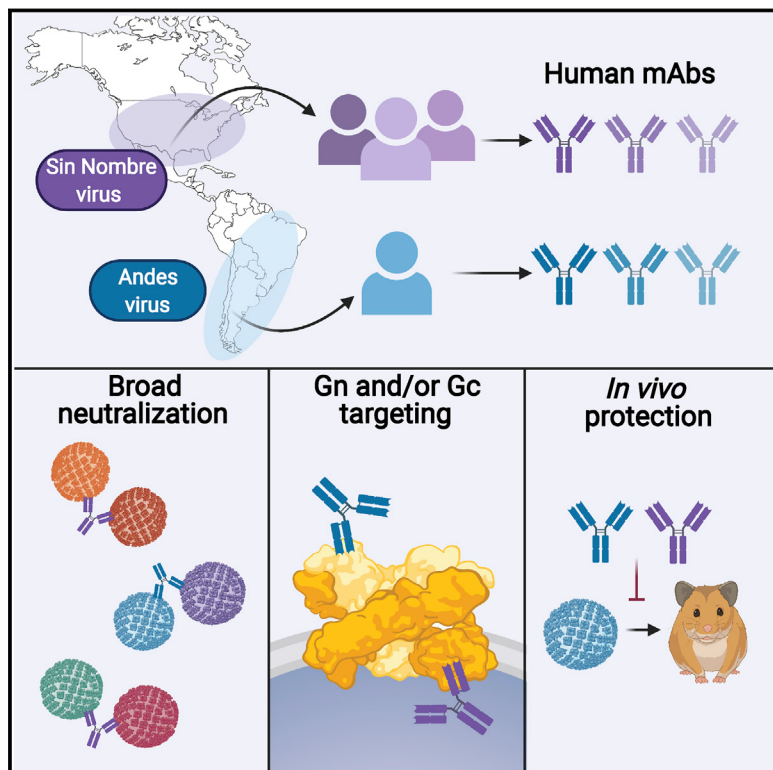


Cell Reports

Article

Broad and potently neutralizing monoclonal antibodies isolated from human survivors of New World hantavirus infection

Graphical abstract



Authors

Taylor B. Engdahl, Natalia A. Kuzmina, Adam J. Ronk, ..., Jay W. Hooper, Alexander Bukreyev, James E. Crowe, Jr.

Correspondence

alexander.bukreyev@utmb.edu (A.B.),
james.crowe@vumc.org (J.E.C.)

In brief

Engdahl et al. show that monoclonal antibodies isolated from human survivors of New World hantavirus infection display broad and potent neutralization across hantavirus species and recognize distinct sites on the glycoprotein spike. Multiple antibodies demonstrate potential therapeutic candidates for New World hantavirus infection. Some antibodies also neutralized Old World hantaviruses.

Highlights

- Hantavirus antibodies were isolated from Sin Nombre/Andes virus infection survivors
- Two antibodies exhibit potent neutralization of both New and Old World species
- Antibodies recognize diverse antigenic sites on the surface of glycoproteins Gc and Gn
- Antibodies protect against Andes virus challenge in hamsters



Article

Broad and potently neutralizing monoclonal antibodies isolated from human survivors of New World hantavirus infection

Taylor B. Engdahl,¹ Natalia A. Kuzmina,^{2,6} Adam J. Ronk,^{2,6} Chad E. Mire,^{5,6,8} Matthew A. Hyde,⁸ Nurgun Kose,³ Matthew D. Josley,⁹ Rachel E. Sutton,³ Apoorva Mehta,³ Rachael M. Wolters,¹ Nicole M. Lloyd,^{2,6} Francisca R. Valdivieso,⁴ Thomas G. Ksiazek,^{2,5,6} Jay W. Hooper,⁹ Alexander Bukreyev,^{2,5,6,*} and James E. Crowe, Jr.^{1,3,7,10,*}

¹Department of Pathology, Microbiology, and Immunology, Vanderbilt University Medical Center, Nashville, TN 37232, USA

²Department of Pathology, University of Texas Medical Branch, Galveston, TX 77555, USA

³Vanderbilt Vaccine Center, Vanderbilt University Medical Center, Nashville, TN 37232, USA

⁴Programa Hantavirus, Instituto de Ciencias e Innovación en Medicina (ICIM), Facultad de Medicina, Clínica Alemana Universidad del Desarrollo, Santiago 7590943, Chile

⁵Department of Microbiology and Immunology, University of Texas Medical Branch, Galveston, TX 77555, USA

⁶Galveston National Laboratory, Galveston, TX 77550, USA

⁷Department of Pediatrics, Vanderbilt University Medical Center, Nashville, TN 37232, USA

⁸Animal Resource Center, University of Texas Medical Branch, Galveston, TX 77555, USA

⁹Virology Division, US Army Medical Research Institute of Infectious Diseases, Fort Detrick, MD 21702, USA

¹⁰Lead contact

*Correspondence: alexander.bukreyev@utmb.edu (A.B.), james.crowe@vumc.org (J.E.C.)

<https://doi.org/10.1016/j.celrep.2021.109086>

SUMMARY

New World hantaviruses (NWHs) are endemic in North and South America and cause hantavirus cardiopulmonary syndrome (HCPS), with a case fatality rate of up to 40%. Knowledge of the natural humoral immune response to NWH infection is limited. Here, we describe human monoclonal antibodies (mAbs) isolated from individuals previously infected with Sin Nombre virus (SNV) or Andes virus (ANDV). Most SNV-reactive antibodies show broad recognition and cross-neutralization of both New and Old World hantaviruses, while many ANDV-reactive antibodies show activity for ANDV only. mAbs ANDV-44 and SNV-53 compete for binding to a distinct site on the ANDV surface glycoprotein and show potently neutralizing activity to New and Old World hantaviruses. Four mAbs show therapeutic efficacy at clinically relevant doses in hamsters. These studies reveal a convergent and potently neutralizing human antibody response to NWHs and suggest therapeutic potential for human mAbs against HCPS.

INTRODUCTION

Hantaviruses are members of the order *Bunyavirales* and are globally emerging pathogens transmitted by rodents to humans (Plyusnin et al., 1996). Hantaviruses are endemic in many regions worldwide and categorized into two groups based on geography and pathobiology. New World hantaviruses (NWH), including Andes virus (ANDV) and Sin Nombre virus (SNV), cause hantavirus cardiopulmonary syndrome (HCPS) with a case fatality rate up to 40% (Kruger et al., 2015; Morens and Fauci, 2020). Hantaviruses are transmitted mainly through the inhalation of aerosolized rodent excreta; however, recent outbreaks of ANDV infection have also included human-to-human transmission through prolonged, direct contact with infected individuals (Alonso et al., 2020; Martinez et al., 2005; Martínez et al., 2020). Old World hantaviruses (OWH), including Hantaan (HTNV), Puumala (PUUV), Dobrava-Belgrade (DOBV), and Seoul (SEOV), cause hemorrhagic fever with renal syndrome (HFRS), with a 1%–15% case fatality

rate (Kruger et al., 2015). There are currently no US Food and Drug Administration (FDA)-approved biologics or other therapeutics for hantavirus infection; however, clinical trials testing the efficacy of M segment (encoding Gn and Gc proteins)-based DNA vaccines have commenced (Boudreau et al., 2012; Brocato et al., 2013; Custer et al., 2003; Hooper et al., 2001a, 2008, 2014a, 2014b). Human monoclonal antibodies (mAbs) isolated from the B cells of ANDV infection survivors have shown therapeutic efficacy in animal models of lethal disease, and murine mAbs derived from B cells of immunized mice also demonstrated efficacy in similar models (Duehr et al., 2020; Garrido et al., 2018). Finally, clinical research has shown that the induction of high titers of neutralizing antibodies in the serum of human patients correlated with increased survival from NWH infection (Bharadwaj et al., 2000). Thus, a robust humoral immune response is critical for surviving NWH infection, but the molecular and genetic basis for human neutralizing antibody responses to NWH is poorly characterized.



Hantavirus-neutralizing antibodies are elicited against the surface glycoprotein spike, a tetrameric complex composed of envelope glycoproteins Gn and Gc (Huiskonen et al., 2010; Li et al., 2016). Gn forms a square-shaped complex at the distal end of the spike and is proposed to play a role in viral attachment and fusion control (Serris et al., 2020). Gc is a class II fusion protein that changes conformation under low pH in the late endosome and induces fusion of the viral and host membranes (Allen et al., 2018; Guardado-Calvo et al., 2016; Willensky et al., 2016). Gc is located proximal to the membrane and is shielded partially by Gn; thus, it may be under less humoral immune pressure, especially in the region of the highly conserved fusion loop (Li et al., 2016; Serris et al., 2020). B cell epitopes have been mapped through peptide scanning to Gn and Gc, although it is currently unknown which epitopes are immunodominant or correspond to recognition by antibodies with neutralizing activity (Arikawa et al., 1989; Engdahl and Crowe, 2020; Heiskanen et al., 1999; Koch et al., 2003).

Broadly neutralizing antibodies (bnAbs) have been characterized for numerous viral families, including coronaviruses (Wec et al., 2020), alphaviruses (Fox et al., 2015; Powell et al., 2020b), influenza viruses (Bangaru et al., 2019; Corti et al., 2011), and ebolaviruses (Flyak et al., 2018; Wec et al., 2016). However, few studies have characterized cross-neutralizing immunity to hantavirus infection (Bharadwaj et al., 2000; Chu et al., 1995; Li et al., 2016; Lundkvist et al., 1997; Tischler et al., 2005). Serological studies of HFRS patient sera have demonstrated modest neutralizing activity for at least two OWHs, while most HCPS patient sera exhibited neutralizing activity for diverse OWHs and NWHs (Chu et al., 1995; Lundkvist et al., 1997). Previous studies of candidate DNA vaccines for the M genome segment from different hantaviruses have demonstrated the importance of the humoral immune response to the surface glycoproteins (Hooper et al., 2014b). Cross-reactivity and cross-protection have been evaluated in the setting of experimental DNA vaccination in animals, but the constructs tested to date did not elicit a broadly neutralizing antibody response (Boudreau et al., 2012; Brocato et al., 2013; Custer et al., 2003; Hooper et al., 2001a, 2014b). Also, murine mAbs have been generated against HTNV Gc protein, which exhibited cross-reactive binding to other OWH species, but they did not possess cross-neutralizing activity (Arikawa et al., 1989; Wang et al., 1993). Studies of human mAbs to SNV have not been published to date, and there is little known about hantavirus bnAbs.

In this study, we isolated a panel of 20 mAbs from three human individuals who were previously infected with SNV and 16 mAbs from one human donor previously infected with ANDV. The results demonstrate that NWH infection induces memory B cells encoding mAbs that recognize a diversity of antigenic sites, display a breadth of binding and neutralizing activity, and mediate *in vivo* therapeutic efficacy against lethal challenge in an animal model of ANDV infection. Specifically, mAbs isolated from SNV-infected individuals were generally broadly neutralizing, while the mAbs isolated from the ANDV-infected individual were generally ANDV specific. ANDV and SNV mAbs recognized eight distinct sites on the hantavirus glycoprotein spike and demonstrated overlap in antigenic site recognition. Four mAbs

tested in a stringent lethal ANDV animal model showed post-exposure protection at a low antibody dose.

RESULTS

Isolation of NWH-reactive mAbs

We isolated a panel of 20 SNV-reactive mAbs from the peripheral blood mononuclear cells (PBMCs) of three otherwise healthy human individuals who previously had suffered symptomatic laboratory-confirmed infection with SNV. Individual 1 was infected in December 2010, and samples were collected in July 2018; individual 2 was infected in June 2017, and samples were collected in June 2018; individual 3 was infected at an unknown date, and samples were collected in April 2018. We also isolated a panel of 16 ANDV-reactive mAbs from a donor previously infected with ANDV. The ANDV-immune donor was infected in December 2006, and the blood sample was collected in Chile in 2015. All of the mAbs were generated through a B cell hybridoma method, as described previously (Alvarado and Crowe, 2016; Powell et al., 2020a; Smith and Crowe, 2015; Yu et al., 2008). We identified B cells expressing ANDV- or SNV-reactive mAbs by screening for binding to ANDV or SNV glycoproteins expressed on the surface of Expi293F cells and detecting NWH-reactive antibodies through flow cytometry on the IQue Screener Plus (Intellicyt). RNA-encoding antibody genes were reverse transcribed, amplified, and sequenced from cloned hybridoma cell lines to identify antibody variable genes for each clone (Tables S1 and S2). Most of the antibodies were of the immunoglobulin G1 (IgG1) isotype, except for SNV-57, which was of the IgG2 isotype.

NWH-reactive mAbs exhibit diverse patterns of neutralization potency and cross-reactivity

We next sought to characterize the ability of our panel of NWH-reactive mAbs to bind and neutralize NWH strains. Most hantaviruses are categorized as Centers for Disease Control and Prevention (CDC) Risk Group 3 pathogens, which require biosafety level 3 (BSL-3) biocontainment for manipulations with authentic viruses. To screen the mAb panel for neutralizing activity in a BSL-2 environment, we used a well-characterized virus pseudotyping system based on vesicular stomatitis virus (VSV) (Higa et al., 2012; Ray et al., 2010; Schnell et al., 1996; Whitt, 2010). In this system, the gene encoding the VSV glycoprotein is removed from the viral genome and replaced with cDNA-encoding green fluorescent protein (GFP), and virions are pseudotyped with NWH glycoproteins Gn and Gc to produce replication-incompetent virus particles. Initially, we tested mAbs for neutralizing activity to pseudotyped (p)VSV/SNV or pVSV/ANDV by detecting a reduction in the number of GFP⁺ cells following the inoculation of cells with pseudotyped particles that had been incubated with mAbs. All of the mAbs that showed neutralizing activity against pVSVs then were tested for the neutralization of authentic SNV strain SN77734 or authentic ANDV strain Chile-9717869 in a plaque reduction neutralization test (PRNT) performed under BSL-3 containment. MAbs were grouped based on neutralization potency for the homologous hantavirus species in PRNT assays (Figures 1A and 1B). Group 1 mAbs showed ultra-potent neutralizing activity (half-maximal inhibitory

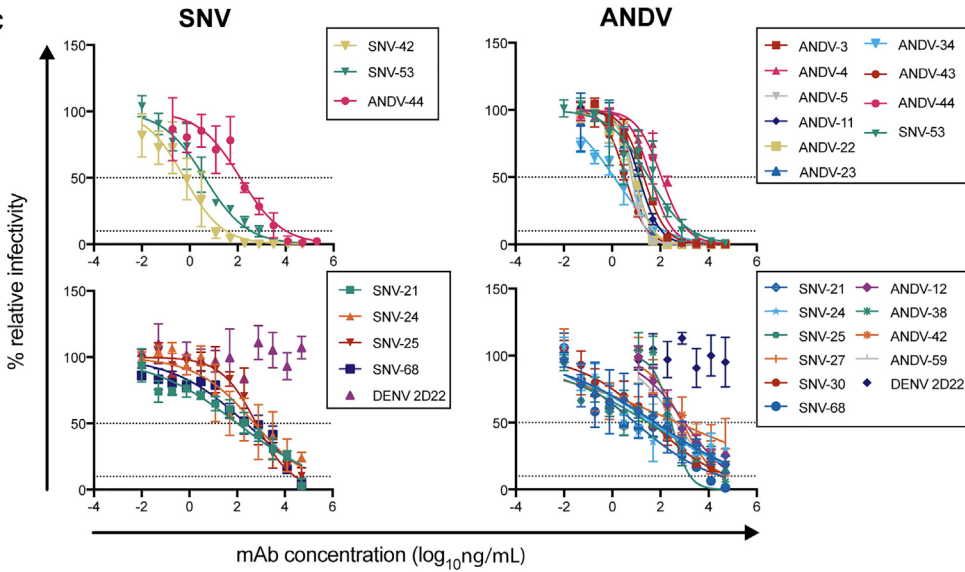
A

Group	mAb	Neutralization						SNV IC ₅₀ (ng/mL)	ANDV IC ₅₀ (ng/mL)	PCDH-1 blocking (%)	Fusion index (%)				
		IC ₅₀ (ng/mL)		IC ₅₀ (ng/mL)		SNV									
		SNV	pVSV/ SNV	ANDV	pVSV/ ANDV	SNV	ANDV								
1	SNV-42	2.4	5.1	NT	>	28	NT	SNV IC ₅₀ (ng/mL)	ANDV IC ₅₀ (ng/mL)	PCDH-1 blocking (%)	Fusion index (%)				
2	SNV-53	21	10	110	8.8	406	1,987								
3	SNV-24	1,156	3.7	3,249	17	>	>								
	SNV-68	1,172	9.1	1,593	15	>	>								
	SNV-21	1,262	8.6	7,065	473	>	>								
	SNV-25	6,980	7.5	1,220	23	>	>								
4	SNV-3	>	28	>	>	>	>								
	SNV-27	>	664	528	47	>	>								
	SNV-30	>	86	1,894	49	>	>								
	SNV-36	>	6.2	>	8.7	>	>								
	SNV-45	>	2,028	>	1,005	>	>								
	SNV-50	>	65	>	6,538	>	>								
	SNV-56	>	>	NT	>	>	NT								
	SNV-57	>	7.1	>	19	>	>								
	SNV-62	>	156	>	68	>	>								
	SNV-67	>	175	>	97	>	>								
	SNV-32	NT	1,693	>	1,483	NT	>								
	SNV-39	NT	>	NT	>	NT	NT								
	SNV-65	NT	>	NT	>	NT	NT								
	SNV-66	NT	>	NT	>	NT	NT								

B

Group	mAb	Neutralization						EC ₅₀ (ng/mL) ANDV Gn/Gc	EC ₅₀ (ng/mL) SNV Gn/Gc	PCDH-1 blocking (%)	Fusion index (%)				
		IC ₅₀ (ng/mL)		IC ₅₀ (ng/mL)		ANDV									
		ANDV	pVSV/ ANDV	SNV	pVSV/ SNV	ANDV	SNV								
1	ANDV-34	1.2	14	NT	>	152	NT	4.5	14	130	22				
	ANDV-5	3.3	3.0	NT	>	16	NT								
	ANDV-43	3.9	2.3	>	>	43	>								
	ANDV-22	5.7	2.3	NT	>	65	NT								
	ANDV-11	6.8	28	NT	>	66	NT								
2	ANDV-23	8.6	17	NT	>	142	NT	9	1,086	157	7				
	ANDV-44	21	0.9	128	>	203	>								
	ANDV-3	38	24	NT	>	884	NT								
3	ANDV-4	68	39	NT	>	1,723	NT	11	13	128	5				
	ANDV-38	380	129	NT	>	>	NT								
	ANDV-42	504	1,423	NT	>	>	NT								
4	ANDV-12	663	17	NT	4.8	>	NT	18	18	133	19				
	ANDV-59	1,008	721	>	>	>	>								
	ANDV-2	>	39	NT	55	>	NT								
	ANDV-54	NT	>	NT	>	NT	NT	3.7	34	119	21				
	ANDV-69	NT	>	NT	>	NT	NT								

C



(legend on next page)

concentration [IC_{50}] < 10 ng/mL), group 2 mAbs showed potent neutralizing activity (IC_{50} 10–100 ng/mL), group 3 mAbs showed a lesser neutralizing activity (IC_{50} 100–10,000 ng/mL), and group 4 mAbs lacked detectable neutralizing activity.

Only one SNV-reactive mAb (SNV-42) demonstrated ultra-potent neutralizing activity, and one mAb (SNV-53) had potent neutralizing activity to authentic SNV (Figure 1A). Four additional mAbs in the SNV-reactive panel also neutralized SNV, while the rest of the mAbs had no detectable neutralizing activity. We also tested the binding of mAbs to the heterologous glycoproteins from ANDV and found that most of the mAbs isolated from SNV-immune individuals also reacted to ANDV glycoproteins and neutralized pVSV/ANDV (Figures 1A, S1, and S2). All of the mAbs that showed cross-reactivity and cross-neutralization of pVSV/ANDV were tested for neutralization of authentic ANDV in a PRNT, and seven of the SNV-reactive mAbs showed neutralizing activity for ANDV.

ANDV-reactive mAbs isolated from the ANDV-immune individual showed limited cross-neutralizing activity, in contrast to the cross-reactive phenotype observed for SNV-reactive mAbs (Figures 1B, S1, and S2). Most of the ANDV-reactive mAbs showed similar neutralization activity in the pVSV/ANDV and authentic ANDV assays, with six mAbs showing ultra-potent neutralizing activity, three mAbs showing potent neutralizing activity, and four mAbs showing a lesser neutralizing activity. Only one mAb tested, ANDV-44, showed neutralizing activity for authentic SNV. Cross-reactivity to SNV Gn and Gc proteins also was limited to five mAbs tested (ANDV-44, -12, -59, -2, and -54).

We noted two distinct functional patterns, complete or incomplete neutralization, for mAbs that showed neutralizing activity to authentic ANDV and SNV (Figure 1C). Incompletely neutralizing mAbs failed to fully neutralize virus (>10% relative infectivity) at the highest concentrations tested. Only three mAbs (SNV-42, SNV-53, and ANDV-44) in group 1 and group 2 showed complete neutralizing activity for SNV (Figure 1C, top left), while the remaining mAbs in group 3 did not show complete neutralization at the

highest concentrations tested (Figure 1C, bottom left). All group 1 and group 2 ANDV-reactive mAbs and SNV-53 showed complete neutralization of ANDV (Figure 1C, top right). mAbs in group 3 showed incomplete neutralization for ANDV at the highest concentrations tested (Figure 1C, bottom right). In summary, most of the ANDV-reactive mAbs showed potent and species-specific neutralizing activity, while SNV-reactive mAbs demonstrated less potent neutralizing activity but greater breadth.

Neutralizing NWH mAbs demonstrate receptor blocking and fusion inhibition activity

To determine the mechanistic basis of neutralization, we tested all mAbs for activity in two *in vitro* assays measuring receptor blocking and fusion inhibition. Protocadherin-1 (PDCH-1) was identified previously as a candidate receptor for NWHs, and extracellular cadherin repeat 1 (EC-1) showed direct binding interactions with ANDV or SNV glycoproteins (Jangra et al., 2018). Therefore, we tested SNV-reactive and ANDV-reactive mAbs for blocking the NWH interactions through a competition-binding assay using soluble EC-1 (sEC-1) protein. Three of the SNV-reactive mAbs (SNV-30, -62, and -67) and four of the ANDV-reactive mAbs (ANDV-3, -5, -38, and -42) showed receptor blocking activity ($\leq 50\%$ residual binding) (Figures 1A and 1B). We only detected binding of sEC-1 to ANDV-transfected cells; thus, SNV-specific mAbs (SNV-3 and SNV-42) were not tested for receptor-blocking activity.

Vero cells expressing the ANDV or SNV surface proteins Gn/Gc undergo cell-to-cell fusion when exposed to acidic (pH 5.5) medium (Bignon et al., 2019; Guardado-Calvo et al., 2016). To test viral fusion *in vitro*, we performed a fusion inhibition assay by adding 10 μ g/mL of each mAb to cells before inducing cell-to-cell fusion. We then counted the percentage of multinucleated cells and normalized values to that for a control sample that was not treated with any mAb, to quantify a fusion index (%) (Figure S3). Through this assay, we determined that each of the SNV-reactive mAbs that showed activity in the pVSV neutralization assay also

Figure 1. NWH-reactive mAbs isolated from individuals previously infected with SNV or ANDV exhibit diverse patterns of neutralization potency, cross-reactivity, and mechanisms of neutralization

(A and B) Neutralization potency of SNV-reactive mAbs (A) or ANDV-reactive mAbs (B) to pseudotyped VSV particles (pVSV/SNV or pVSV/ANDV), SNV strain SN77734 (SNV), or ANDV strain Chile-9717869 (ANDV). Antibodies in a dilution series of decreasing concentrations were incubated with pVSVs or authentic virus, the suspension was used to inoculate cells, and then GFP⁺ cells or plaques were counted to determine relative infectivity. IC_{50} or IC_{90} values were obtained using non-linear fit analysis, with the top of the curve constrained to 100 and the bottom of the curve constrained to 0, using Prism software version 7 (GraphPad Software). The colors indicate the relative potency of the antibody. The data shown are average values from 2–3 independent experiments. Binding to proteins for each hantavirus species was determined by flow cytometric analysis. Gn and Gc were displayed on the surface of mammalian cells and incubated with decreasing concentrations of mAb. EC₅₀ binding values were obtained using non-linear fit analysis, with the bottom of the curve constrained to 0, using Prism software. The value for %PE⁺ cells was determined by gating on cells stained only with secondary antibodies. The colors indicate the relative potency of the antibody. > indicates that the neutralization or reactivity was not detected at the highest concentration tested, 20 μ g/mL. NT indicates that the mAb was not tested. The data shown are average values from 3 independent experiments. PCDH-1 blocking (%) was determined through a flow cytometric assay, in which mAbs were added at saturating concentration before the addition of the soluble PCDH-1 domain, sEC-1 labeled with Alexa Fluor 647 dye. PCDH-1 blocking was defined by the reduction of the maximal binding score to <50% of un-competed binding (green boxes). The data shown are average values from 3 independent experiments. The fusion index (%) was determined by adding mAbs to Vero cells transfected with cDNAs encoding SNV or ANDV Gn/Gc, and then inducing fusion through exposure to medium with low pH and counting the percentage of multinucleated cells by fluorescent microscopy. The percentage of multinucleated cells in mAb-treated samples then was divided by the percentage of multinucleated cells in a non-mAb-treated sample (representing maximal fusion index). Fusion-inhibiting mAbs were defined by the reduction of the maximal fusion index to <50% of non-mAb-treated cells (yellow boxes). The data shown are the average values from 3 independent experiments.

(C) Representative binding curves of neutralizing antibodies mediating complete (top) or incomplete (bottom) neutralization for authentic SNV (left) or ANDV (right). The dotted lines indicate 10% or 50% relative infectivity. The data shown are average values for technical replicates \pm SDs. The experiment was performed 2–3 times independently with similar results; one experiment is shown.

See also Figures S1–S3 and Tables S1 and S2.

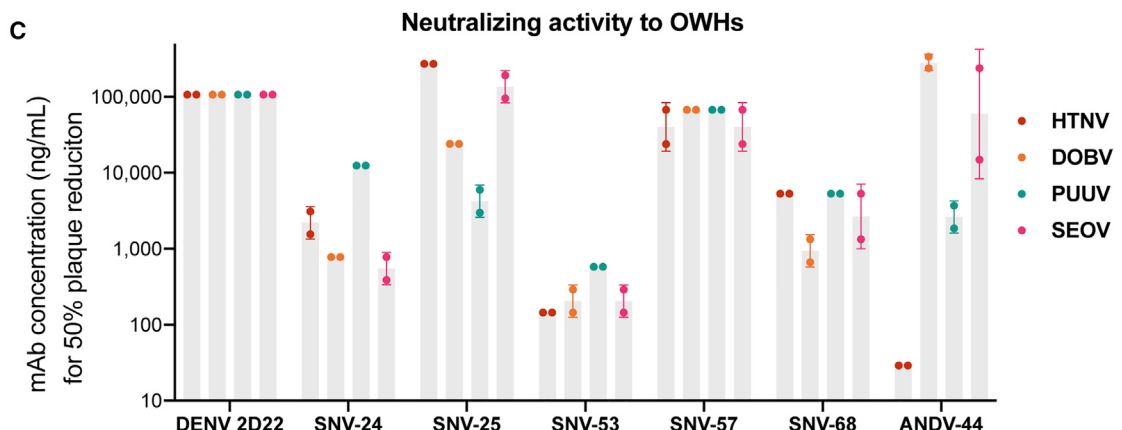
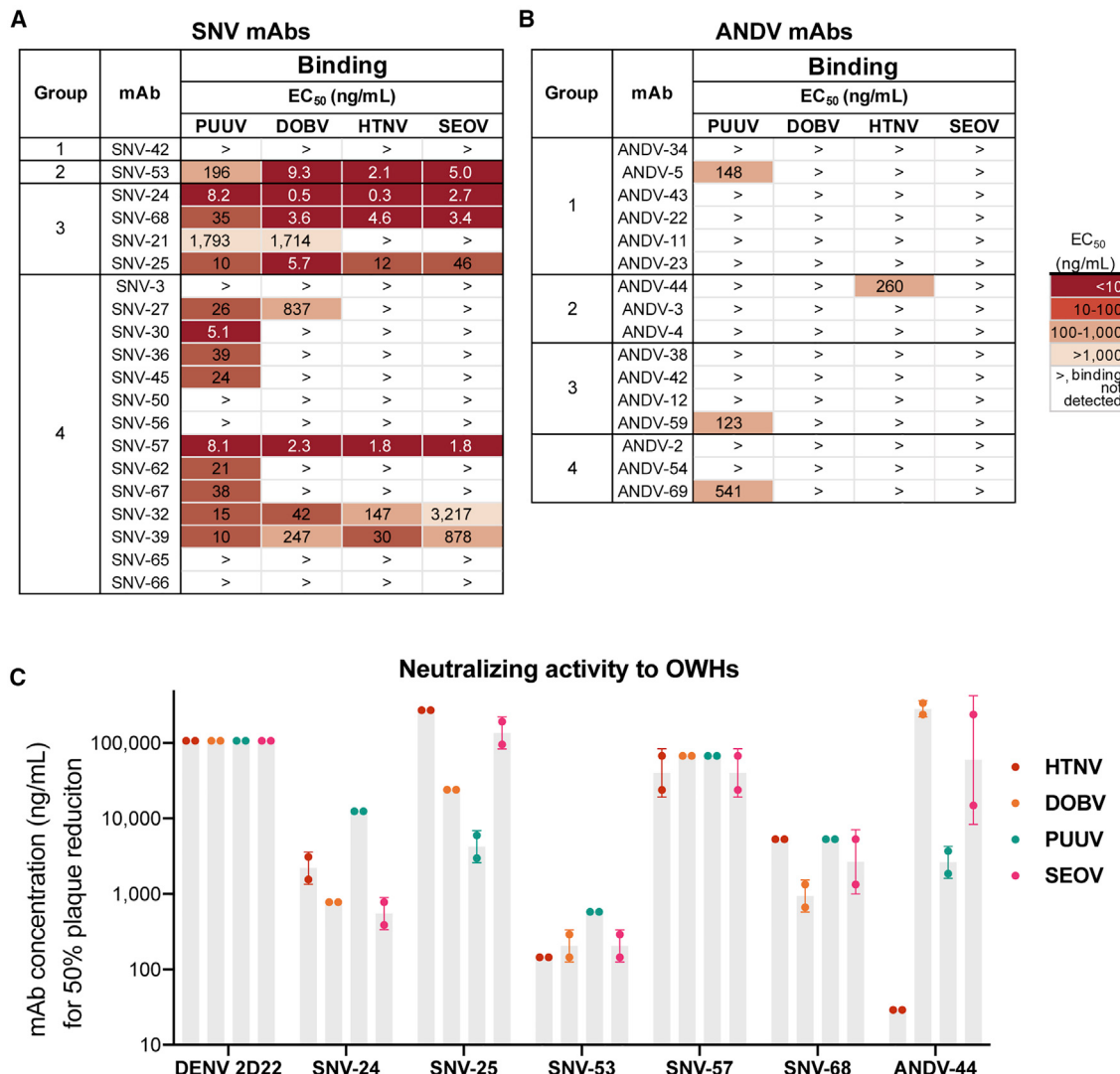


Figure 2. NWH-reactive mAbs show binding and neutralizing activity against OWH species

(A and B) Binding potency of mAbs isolated from SNV-immune (A) or ANDV-immune (B) human individuals for four OWH species: Puumala (PUUV), Dobrava-Belgrade (DOBV), Hantaan (HTNV), and Seoul (SEOV). EC₅₀ binding values were obtained using non-linear fit analysis, with the bottom of curve constrained to 0, using Prism software. The data are shown as average values from 3 independent experiments. The colors indicate the relative potency of the antibody. > indicates no detectable reactivity at concentrations >20 µg/mL.

(C) Neutralization potency of broadly reactive mAbs to HTNV strain 76-118, DOBV strain Dobrava, PUUV strain K27, or SEOV strain SR-11. Neutralization potency was determined with a plaque reduction neutralization assay. The neutralizing mAb concentration indicates the concentration at which there was a ≥50% reduction in plaque count by each mAb. The data shown are average values for technical replicates ± SDs. The experiments were performed 2–3 times independently with similar results.

See also Figures S1 and S2.

showed a reduction in cell-to-cell fusion (Figures 1A and 1B). In addition, all of the ANDV-reactive mAbs in group 1 and group 2 showed fusion-inhibiting activity. Thus, NWH mAbs showed a range of receptor-blocking and fusion-inhibiting activities *in vitro*, and most of the neutralizing antibodies also inhibited fusion.

NWH-reactive mAbs show binding and neutralizing activity against OWH species

Since many of the mAbs cross-reacted with SNV and ANDV, we sought to determine the breadth of binding and neutralizing

activity to OWHs from different species. To that aim, we transiently transfected Expi293F cells to surface display the glycoproteins from PUUV, DOBV, HTNV, and SEOV and tested the reactivity of all mAbs in the panel (Figures 2A, 2B, and S1). Seven of the SNV-reactive mAbs showed reactivity to all four OWHs tested (Figure 2A). Each of the broadly reactive mAbs also was tested for, but did not demonstrate, detectable binding to unrelated mammalian cell surface-displayed eastern equine encephalitis virus (EEEV) E1/E2 proteins or Rift Valley fever virus (RVFV) Gn/Gc proteins (data not shown); thus, these mAbs are likely

broadly reactive between representatives of the *Hantavirus* genus only. We also generated pVSVs bearing Gn and Gc from OWHs Puumala (pVSV/PUUV), Dobrava-Belgrade (pVSV/DOBV), Hantaan (pVSV/HTNV), and Seoul (pVSV/SEOV) to screen for broad neutralizing activity (Figure S2). Five SNV-reactive mAbs showed broad neutralizing activity in the surrogate assays, and thus we tested for neutralizing activity to authentic OWHs in a plaque reduction neutralization test (Figure 2C). SNV-24 and SNV-68 reduced the infectivity of DOBV by 50% at <1 µg/mL, and SNV-24 also reduced infectivity of SEOV by 50% at 551 ng/mL. SNV-53 reduced infectivity of all four tested OWHs by 50% at <1 µg/mL.

In contrast, most of the ANDV-reactive mAbs did not show detectable reactivity or neutralizing activity for OWHs (Figure 2B). Only three mAbs (ANDV-5, -59, and -69) showed reactivity to PUUV, but these mAbs did not have any detectable neutralizing activity for pVSV/PUUV (Figure S2). ANDV-44 is the only mAb isolated from the ANDV-immune donor that showed detectable reactivity to HTNV, and exhibited potent neutralizing activity to authentic HTNV (Figure 2C). The neutralization potency of ANDV-44 was beyond the lower limit of the assay, and thus ANDV-44 showed a 50% reduction in HTNV infectivity at <29 ng/mL. These results demonstrate that the SNV-reactive mAbs show broad reactivity and neutralizing activity to OWHs, while the ANDV-reactive mAbs we isolated are generally species specific.

At least eight major antigenic sites on Gn or Gc are recognized by NWH-reactive mAbs

We next sought to determine the number of major antigenic sites recognized by human mAbs elicited during infection with NWHs, especially the sites on Gn and Gc recognized by the potently neutralizing mAbs. To determine the patterns of binding, we used a flow cytometric-based competition-binding analysis on ANDV glycoproteins (Figure 3A). Antibodies were clustered based on competition with other mAbs; thus, mAbs binned together likely bind to the same antigenic site. The data revealed that mAbs in the two panels can be classified based on their binding sites, and there were eight different antigenic sites targeted by mAbs in the two panels. Over half of the SNV-reactive mAbs resided in one major group (designated site A1), primarily representing broad, incompletely neutralizing mAbs, while non-neutralizing SNV-reactive mAbs binned in a separate competition group (site E). Ultra-potently neutralizing ANDV-reactive mAbs binned into three distinct sites (sites C1, D, and F). SNV-reactive and ANDV-reactive antibodies generally binned into separate competition-binding groups. However, there was overlap for two sites, A and C. Site C1 contained potently neutralizing and cross-reactive mAbs (SNV-53 and ANDV-44), while site C2 contained cross-reactive but weakly neutralizing or non-neutralizing mAbs (SNV-21, ANDV-2, and ANDV-12). Overlap also occurred between sites A1 and A2, in which non-neutralizing mAb SNV-50 competed with weakly neutralizing, cross-reactive mAb ANDV-59. SNV-reactive receptor-blocking mAbs competed with each other (site A1), and ANDV-reactive receptor-blocking mAbs also competed with each other (site F), although these sites did not overlap. We did not determine binding sites for mAbs SNV-42 and SNV-3 on ANDV glycoproteins.

However, SNV-42 and SNV-3 bin into a distinct group when competed against the other SNV-reactive mAbs (data not shown). Based on the competition-binding groups, potently neutralizing and broadly reactive mAbs target multiple epitopes, and two cross-reactive sites exist for ANDV and SNV that are recognized by human B cells.

We also tested the binding of mAbs to Gn or Gc proteins individually (Figure 3B). Site A1 contained mAbs that bound to Gc, while sites B, D, E, and F contained mAbs that bound to Gn. SNV-specific mAbs SNV-3 and SNV-42 also bound to Gn. MAbs in sites A2, C1, and C2 did not show detectable reactivity to Gn or Gc.

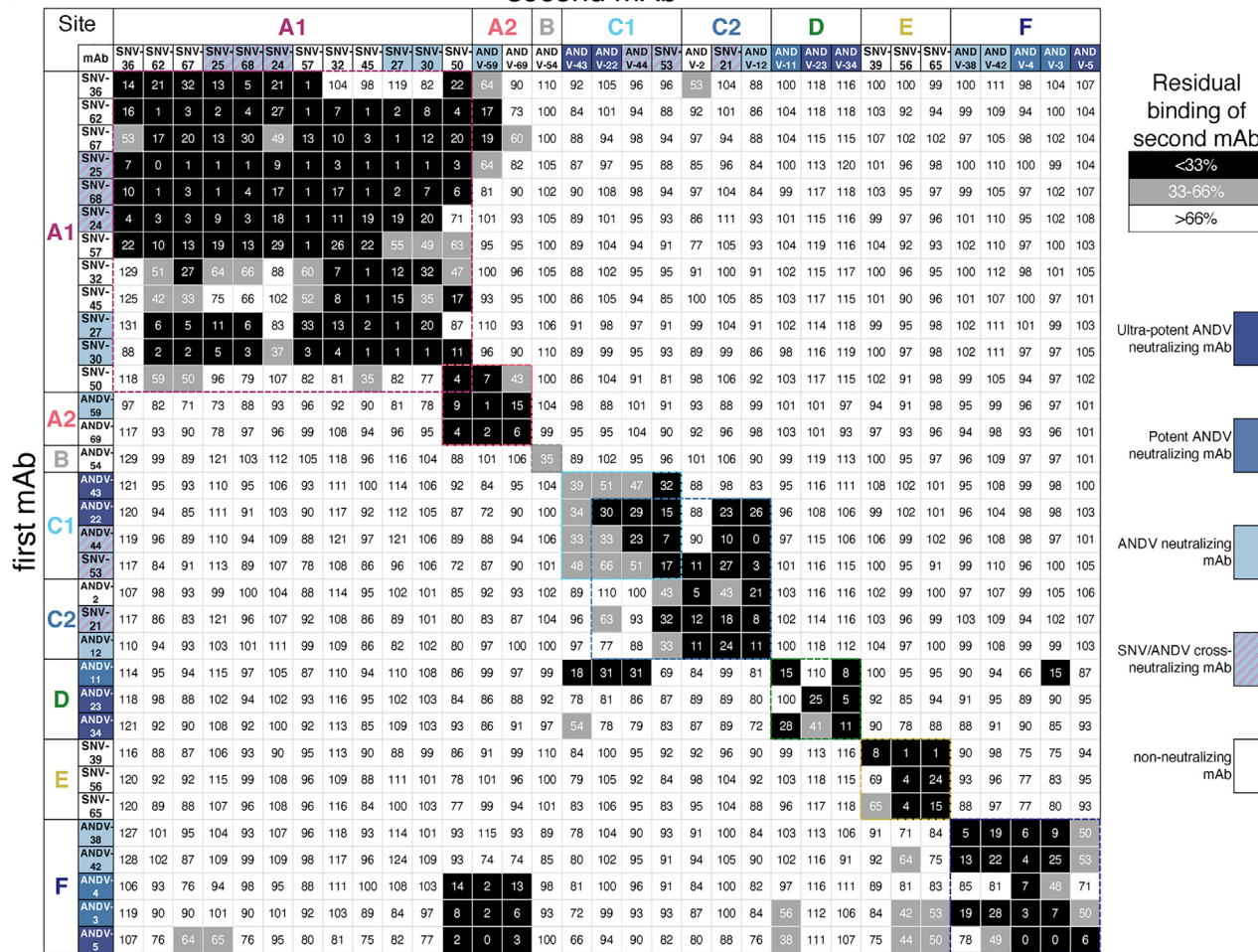
Four NWH mAbs protect Syrian hamsters in ANDV challenge

To determine whether mAbs in the panel have therapeutic efficacy in a post-exposure administration, we tested a subset of five mAbs in the golden Syrian hamster model of ANDV infection. The golden Syrian hamster is the preferred animal model for hantavirus infection, and ANDV is the only NWH that causes lethal disease in immunocompetent hamsters with clinical signs and pathobiological features similar to human disease (Hooper et al., 2001b; Wahl-Jensen et al., 2007). We chose several mAbs for animal protection studies based upon their *in vitro* neutralizing characteristics, competition mapping, and breadth of reactivity. One ANDV-specific mAb in group 1 (ANDV-5) and one cross-neutralizing mAb from group 2 (ANDV-44) were chosen from the ANDV-reactive panel. One cross-neutralizing mAb from group 2 (SNV-53), one cross-neutralizing mAb from group 3 (SNV-24), and one incomplete neutralizing mAb from group 4 (SNV-30) were chosen from the SNV-reactive panel. Hamsters ($n = 6$ per treatment group) were inoculated with 200 PFU ANDV via the intramuscular (i.m.) route and then were injected via the intraperitoneal (i.p.) route with 5 mg/kg of either recombinant (r)SNV-30, rSNV-24, rSNV-53, rANDV-5, rANDV-44, or a control antibody rDENV 2D22 on days 3 and 8 post-infection (p.i.). All of the animals in the control group started displaying illness beginning on day 9 p.i., and all of them succumbed or were moribund and were euthanized by day 11 p.i. Three of the animals treated with rSNV-30 succumbed or were euthanized by day 10 p.i., two of the animals treated with rSNV-24 or rANDV-5 were euthanized by day 11 p.i., and only one animal treated with rSNV-53 succumbed at day 10 p.i. (Figure 4A).

All of the animals treated with rANDV-44 survived the challenge and showed a reduction in overall lung histopathology at necropsy (Figure S4A). Gross pathology in lungs collected from animals treated with control antibody showed clear signs of inflammatory changes in all or nearly all visible tissue, including significant vascular congestion and desquamation of airway epithelia. Lungs from rANDV-44-treated animals did not show any external signs of pathology, reduced congestion, or airway changes (Figures S4B and S4C). We observed vascular leakage in several animals, which was reduced in rANDV-44-treated animals.

Since the progression of clinical signs in the animals was very rapid, we could not detect any significant weight loss in any group (Figure 4B). Lungs and livers were collected from moribund animals and from animals that survived the

A second mAb



B

Site	A1												A2				B			C1			C2			D			E			F			SNV-specific	
mAb	SNV-36	SNV-62	SNV-67	SNV-25	SNV-68	SNV-24	SNV-57	SNV-32	SNV-45	SNV-27	SNV-30	SNV-50	AND-V-59	AND-V-69	AND-V-54	AND-V-43	AND-V-22	AND-V-44	AND-SNV-53	AND-V-21	AND-V-12	AND-V-11	AND-V-23	AND-V-34	SNV-39	SNV-56	SNV-65	AND-V-38	AND-V-42	AND-V-4	AND-V-3	AND-V-5	SNV-3	SNV-42		
Gn	>	>	>	>	>	>	>	>	>	>	>	>	>	>	>	106	>	>	>	>	>	>	36	1.9	16	3.9	7.0	8.0	12	3.9	204	132	8.0	24	2.3	
Gc	35	60	81	22	45	67	41	168	49	24	82	23	>	>	>	>	>	>	>	>	>	>	>	>	>	>	>	>	>	>	>	>	>	>	>	

Figure 3. NWH-reactive mAbs bind to at least eight major antigenic sites on Gn or Gc based on competition-binding analysis

(A) Unlabeled antibodies were incubated with Expi293F cells transfected with cDNA encoding ANDV Gn/Gc at saturating concentrations and then competed with a second antibody labeled with Alexa Fluor 647. Percent competition was analyzed and quantified using flow cytometry as compared to the un-competed binding of the second mAb. Competing antibodies were defined as those with <33% of the maximal un-competed binding in the presence of an unlabeled first antibody (black). Non-competing antibodies were defined as those with >66% of the maximal un-competed binding (white). Intermediate competing antibodies were defined as those with 33%-66% of the maximal un-competed binding (gray). Antibodies are colored based on neutralization potency to ANDV and SNV. Antibodies were clustered based on the Pearson correlation generated relatedness score based on normalized competition values. The values shown are averages from 3 independent experiments.

(B) Binding to Gn displayed on the surface of Expi293F cells was determined using a flow cytometry-based binding assay, as described previously. Binding to recombinant Gc was determined using an ELISA. EC₅₀ binding values were obtained using non-linear fit analysis with the bottom of the curve constrained to 0, using Prism software. The colors indicate the relative potency of the antibody. > indicates that neutralization or reactivity was not detected at the highest concentration tested, 20 µg/mL. The data shown are the average values from 3 independent experiments.

observation period without clinical signs and determined the viral load in these organs. The majority of the animals that succumbed during days 9–11 p.i. had detectable ANDV in their

lungs and liver, while all of the animals that

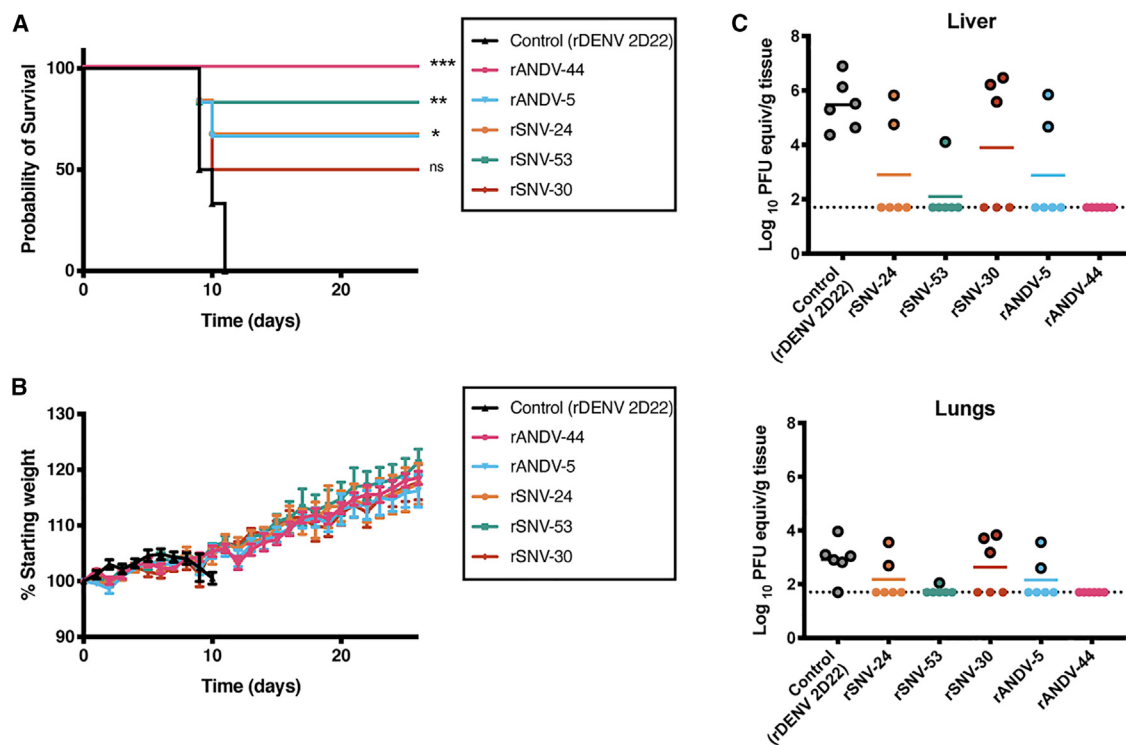


Figure 4. Four NWH mAbs protect Syrian hamsters in ANDV challenge

(A) 8-week-old Syrian hamsters ($n = 6$ per treatment group) were inoculated with 200 PFU of ANDV intramuscularly (i.m.), and 5 mg/kg of indicated mAb was administered intraperitoneally (i.p.) at 3 and 8 dpi. Animals were treated with a dengue-specific mAb (rDENV 2D22) to serve as an isotype control. The statistical analysis was done using a log-rank (Mantel-Cox) test comparing each group to the control (rDENV 2D22); * $p < 0.01$; ** $p < 0.01$; *** $p < 0.001$; ns, non-significant.

(B) Body weight measurements averaged for each treatment group. The data shown are mean \pm S.E.M. for each treatment group.

(C) Lungs and livers were collected upon euthanasia and used to determine viral titer in tissue. Dots with black borders indicate animals that were found dead or

euthanized according to Institutional Animal Care and Use Committee (IACUC) protocol before the termination of the study. The dotted line indicates the limit of detection.

See also Figure S4.

DISCUSSION

Here, we present the isolation and characterization of NWH mAbs from the memory B cells of individuals who had recovered from previous ANDV or SNV infection. Most of the SNV-reactive mAbs targeted Gc and displayed broad reactivity across NWHs and OWHs, but showed weak or non-neutralizing activity to authentic hantaviruses. Conversely, most ANDV-reactive mAbs targeted Gn and had limited breadth of binding to NWHs and OWHs, but demonstrated potent neutralizing activity to ANDV. We demonstrated that the recognition sites for NWH-reactive mAbs map to at least eight distinct antigenic sites on the ANDV glycoprotein spike complex, and multiple sites of vulnerability for cross-reactive neutralization exist on Gn or Gc. Four NWH mAbs were protective for Syrian hamsters infected with ANDV in a very stringent lethal disease model.

We used two different assays to test the neutralization potency of mAbs in the panel. We performed neutralization assays with VSVs pseudotyped with hantavirus glycoproteins under BSL-2 containment and with authentic hantaviruses under BSL-3 containment. Previous studies demonstrated that pVSV hantavirus neutralization assays provide results comparable to those

obtained in PRNT assays with authentic viruses (Higa et al., 2012; Hooper et al., 2014a; Perley et al., 2020). The IC₅₀ neutralizing values in our study were largely similar between the two assays conducted with ANDV-reactive mAbs, but many of the SNV-reactive mAbs that neutralized pVSV failed to neutralize authentic SNV or ANDV. SNV-reactive mAbs were isolated based on binding to SNV Gn/Gc proteins from the SNV strain CC107 displayed on transfected cell surfaces, while the authentic SNV strain tested in neutralization tests was SN77734. Minor sequence variations may account for the differences observed in neutralization between the pVSV and authentic SNV. Also, it is possible that the organization of the Gn/Gc complex expressed on mammalian cells or packaged in VSV particles differs significantly from the organization of those proteins on the surface of authentic SNV virions.

We observed incomplete neutralization and non-sigmoidal dose-response curves with serial dilutions of most SNV mAbs when tested against authentic SNV. This result may stem from the heterogeneity of virions in the suspensions used for neutralization, as hantavirus virions display a diverse range of particle morphologies (Parvate et al., 2019). Some HIV bnAbs also demonstrate distinctive non-sigmoidal neutralization curves

and incomplete (<100%) neutralizing activity (McCoy et al., 2015; Webb et al., 2015). This feature is a characteristic of functional and epitope-specific classes of HIV bnAbs that target the glycan-rich gp41 membrane-proximal external region and may result from the particle heterogeneity of glycosylation when HIV strains are produced in cell culture. Although it is not entirely clear what effect incomplete neutralization has on protective efficacy *in vivo*, as in HIV, it is likely that bnAbs with neutralizing antibody activity slopes >1 show greater therapeutic potential (Webb et al., 2015). Diverse classes of hantavirus antibodies based on differing epitopes or mechanisms of action have not been described to date, and incomplete and non-sigmoidal neutralization may be a characteristic of hantavirus bnAbs. Recent evidence has supported the hypothesis that the hantavirus glycoprotein spike complex “breathes,” exhibiting a movement in which the “open” form of the spike exposes the fusion loop for membrane insertion, but does not undergo the uncappling by Gn necessary to promote viral fusion (Bignon et al., 2019; Serris et al., 2020). This dynamic feature of the spike may expose decoy epitopes on Gc that are the target of weakly neutralizing mAbs. Such an epitope would be occluded in the “closed” form of the spike, and particle heterogeneity in terms of open or closed spike status could account for weak or incomplete neutralization demonstrated by mAbs in this study.

We also tested NWH mAbs for receptor-blocking and fusion-inhibiting activity using *in vitro* assays and showed that most of the neutralizing mAbs inhibited fusion. Only one ultra-potent neutralizing mAb, ANDV-5, blocked binding to the PCDH-1 receptor. Therefore, blocking of PCDH-1 engagement is not the only essential feature of potent NWH neutralization. β 3 integrins also have been shown to facilitate the entry of hantaviruses into host cells, and mAbs may block interactions between viral Gn/Gc and host integrin β 3 to achieve potent neutralization (Gavrilovskaya et al., 1998, 1999, 2010). Further work is required to determine whether potently neutralizing mAbs block other receptor engagements or whether there are other receptors or critical attachment factors that have yet to be identified.

Notably, we observed asymmetric patterns of breadth of binding and neutralization for the mAbs isolated from SNV-immune donors compared to the mAbs isolated from the ANDV-immune donor. Many of the SNV mAbs bound to and neutralized both SNV and ANDV, while most of the ANDV mAbs were specific to ANDV only. These studies provide a snapshot of the pattern of response in those studied. Due to the limited number of individuals studied and mAbs isolated in this study, it is not possible to determine whether the specificity patterns reflected in the panels are generally characteristic of most human ANDV or SNV immune responses. Little is known about the specificity of the human serologic response to hantavirus infection, although cross-neutralizing activity to heterologous hantaviruses has been detected in sera from HFRS or HCPS patients (Chu et al., 1995). Previous work has shown that vaccination with cDNA encoding the SNV M genomic segment failed to protect Syrian hamsters from lethal ANDV challenge and failed to elicit cross-neutralizing antibodies in sera (Hooper et al., 2013). DNA vaccine strategies also have proceeded with a combination of HTNV/PUUV/ANDV/SNV M genes as an experimental candidate pan-hantavirus vaccine to protect against multiple HFRS and HCPS

agents, however, this approach failed to induce neutralizing antibodies for SEOV or DOBV (Hooper et al., 2006, 2013). Thus, it is notable that several of the mAbs isolated in our study showed reactivity and neutralizing activity for the more distantly related OWHs. Broadly neutralizing mAbs SNV-24, SNV-68, and SNV-25 likely bind to a highly conserved epitope on the fusion protein Gc. Gc is located proximal to the membrane and is shielded partially by Gn; thus, it may be under less humoral immune pressure, especially in the region of the highly conserved fusion loop (Li et al., 2016; Serris et al., 2020). A recently published study also demonstrated that a candidate vaccine consisting of PUUV, HTNV, and ANDV antigens induced more Gc-reactive murine antibodies than candidate vaccines containing ANDV antigens only, further suggesting a role of Gc-recognizing mAbs in a broadly reactive humoral response (Duehr et al., 2020).

Interestingly, SNV-53, a broadly neutralizing mAb, and ANDV-44, a potent NWH- and HTNV-neutralizing mAb, did not show reactivity to either Gn- or Gc-soluble proteins. This finding suggests that hantaviruses may contain a conserved site of vulnerability that is only formed or accessible in the quaternary spike structure. Defining the sites targeted by these bnAbs can inform pan-hantavirus vaccine development. These results suggest that immunogens presenting quaternary antigenic sites may be more effective in eliciting a cross-neutralizing antibody response.

It is theoretically possible that weak reactivity and neutralization of multiple hantavirus species by a mAb could lead to antibody-dependent enhancement (ADE) of infection or disease. ADE caused by Fc-region-facilitated uptake into infection-permissive cells bearing FcRs has been a consideration for developing vaccines and therapeutics for some other infectious diseases, especially dengue virus (Katzelnick et al., 2017). Some non-neutralizing influenza virus antibodies mediate the enhancement of respiratory disease (ERD) in certain animal models. However, studies of influenza virus infections in humans, which commonly elicit cross-reactive mAbs to heterologous strains, have not shown any evidence of enhancing influenza disease (Arvin et al., 2020). One study has demonstrated ADE of HTNV infection *in vitro*, but ADE of hantaviral disease in clinical settings has not been reported (Yao et al., 1992). More research should be done to determine the optimal serum neutralizing titers and associated dose of mAb therapy for hantavirus disease, and whether certain antigenic sites on the hantavirus glycoproteins elicit suboptimal humoral responses.

We mapped recognition sites for the NWH-reactive antibodies to eight distinct antigenic sites on the Gn/Gc spike through competition-binding assays using full-length IgG. Analyzing the patterns formed by competition-binding groups and the functional groups assigned by cross-neutralizing potency revealed that most of the ANDV and SNV-reactive mAbs segregated into separate groups. However, four ANDV-reactive mAbs that cross-reacted with SNV (ANDV-2, -12, -44, and -59) did compete for binding with SNV-reactive mAbs and clustered into overlapping competition-binding groups, indicating that there are homologous sites on the glycoprotein spikes of different NWHs recognized by human B cells. These findings indicate that NWH infections can elicit similar classes of neutralizing antibodies that target a homologous site on NWH glycoproteins.

Based on competition-binding analysis, at least one antigenic site on Gc is targeted by most cross-neutralizing antibodies (designated here as antigenic site A1). A recently described co-crystal structure of the PUUV mAb 4G2 in complex with Gc shows that this cross-neutralizing mAb binds to a prefusion, monomeric form of Gc (Rissanen et al., 2020). Antigenic site A1 may be similar to the conserved site targeted by mAb 4G2. Many of the mAbs in this group demonstrated broad but incomplete neutralization of authentic virus; this finding is consistent with the occluded nature of some epitopes on Gc (Li et al., 2016; Rissanen et al., 2020; Serris et al., 2020). The potently neutralizing mAbs we isolated from ANDV-immune donors predominantly targeted Gn. Receptor-blocking ANDV mAbs (recognizing antigenic site F) also bound to Gn, suggesting that the receptor-binding site for PCDH-1 may be located on Gn. Also, it is likely that the potent and cross-neutralizing mAbs SNV-53 and ANDV-44 (recognizing antigenic site C1) that lack detectable binding to Gn or Gc may bind to a quaternary epitope not fully recapitulated in individual recombinant Gc or Gn monomeric protein reagents. Determining the critical antigenic sites targeted during ANDV and SNV infection will be essential for rational vaccine design and the development of effective medical countermeasures against hantaviruses.

Two previous studies tested passive transfer of ANDV neutralizing mAbs in the Syrian hamster challenge model and showed 100% protection with a different, likely less invasive infection route (200 PFU of the virus were delivered intranasally, whereas we used i.m. challenge) and at a substantially higher dose of antibodies at 25 mg/kg (Duehr et al., 2020) or 50 mg/kg (Garrido et al., 2018). In contrast, we showed efficacy of mAbs ANDV-44, ANDV-5, SNV-53, and SNV-24 in a low-dose treatment (5 mg/kg) in a highly lethal model, which supports the potential for the clinical use of these mAbs as therapeutic molecules to treat hantavirus infections at lower doses than previously described.

As evidenced by the coronavirus disease 2019 (COVID-19) pandemic, newly emerging infectious diseases can profoundly affect the world and disproportionately target society's most vulnerable members. Hantaviruses, in particular, thrive on social inequities due to the zoonotic transmission from rodents to humans in low-resource settings. In addition, climate change has been linked to the spillover of hantaviruses from the rodent to the human population and will continue to be an issue as environmental destruction worsens globally (Prist et al., 2016). Our work presents therapeutic candidates for the treatment of NWH-related disease and provides a foundation for further work characterizing the B cell response to hantavirus infection.

STAR★METHODS

Detailed methods are provided in the online version of this paper and include the following:

- KEY RESOURCES TABLE
- RESOURCE AVAILABILITY
 - Lead contact
 - Materials availability
 - Data and code availability

● EXPERIMENTAL MODEL AND SUBJECT DETAILS

- Cell lines
- Human subjects
- Viruses
- Animal model

● METHOD DETAILS

- Generation of cell-surface expressed antigens
- Screening and binding of NWH-reactive antibodies
- Isolation of human hybridomas and purification of monoclonal antibodies
- Antibody gene sequence analysis
- Generation of pseudotyped VSVs
- Pseudotyped virus neutralization assay
- Receptor blocking assay
- Fusion inhibition assay
- Plaque reduction neutralization assay with authentic SNV or ANDV
- Plaque reduction neutralization titer with authentic OWHs
- Competition-binding assay
- Expression and purification of recombinant Gc (rGc) protein and ELISA binding assays
- Expression of cell-surface-displayed Gn protein and binding assay
- Testing of protective efficacy against ANDV in the Syrian hamster model
- Histopathology

● QUANTIFICATION AND STATISTICAL ANALYSIS

- Binding and neutralization curves
- Competition-binding analysis
- Testing of protective efficacy in Syrian hamsters

SUPPLEMENTAL INFORMATION

Supplemental information can be found online at <https://doi.org/10.1016/j.celrep.2021.109086>.

ACKNOWLEDGMENTS

At Vanderbilt, we thank R. Carnahan, P. Gilchuk, S. Zost, and C. Slaughter for intellectual contributions and training and R. Irving and R. Nargi for managerial support. We thank E. Armstrong, J. Rodriguez, C. Gainza, J. Reidy, A. Trivette, and R. Troseth for technical support. We thank M. Leksell, M. Mayo, K. Moton, T. Martin, G. DeBellis, A. Bunnell, and A. Jordan for administrative assistance. We acknowledge the UTMB Animal Resource Center for the animal study's support and thank M. Milazzo at UTMB for facilitating BSL-3 and ABSL-4 training and transferring viral isolates. We acknowledge C. Spiropoulou at the CDC for providing rabbit anti-SNV polyclonal sera. In Chile, we acknowledge A. Cuiza for enrolling the ANDV patients and obtaining the ANDV samples and C. Vial for preparing the PBMCs from ANDV patients. The work of T.B.E. was supported by the NIH (training grant 5T32GM008320-30). This project received support from the Military Infectious Disease Research Program, Program Area T (project MI210048). The graphical abstract was made in part with BioRender.com.

AUTHOR CONTRIBUTIONS

Conceptualization, T.B.E., A.B., and J.E.C.; methodology, T.B.E., A.B., J.W.H., and J.E.C.; investigation, T.B.E., N.A.K., A.J.R., C.E.M., M.A.H., N.K., M.D.J., R.E.S., A.M., R.M.W., and N.M.L.; writing – original draft, T.B.E. and J.E.C.; writing – review & editing, T.B.E., A.B., N.A.K., J.W.H., and J.E.C. (all authors)

edited and approved the final version); funding acquisition, A.B., J.W.H., and J.E.C.; resources, F.R.V.; supervision, A.B., T.G.K., J.W.H., and J.E.C.

DECLARATION OF INTERESTS

J.E.C. has served as a consultant for Eli Lilly, GlaxoSmithKline, and Luna Biologics; is a member of the Scientific Advisory Boards of CompuVax and Meissa Vaccines; and is Founder of IDBiologics. The Crowe laboratory at Vanderbilt University Medical Center has received unrelated sponsored research agreements from Takeda Vaccines, IDBiologics, and AstraZeneca. Vanderbilt University has applied for patents concerning hantavirus antibodies that are related to this work. All of the other authors declare no competing interests. Opinions, interpretations, conclusions, and recommendations contained herein are those of the authors and are not necessarily endorsed by the US Department of Defense.

Received: October 20, 2020

Revised: March 17, 2021

Accepted: April 14, 2021

Published: May 4, 2021; corrected online: July 12, 2021

REFERENCES

- Allen, E.R., Krumm, S.A., Raghwani, J., Halldorsson, S., Elliott, A., Graham, V.A., Koudriakova, E., Harlos, K., Wright, D., Warinwe, G.M., et al. (2018). A protective monoclonal antibody targets a site of vulnerability on the surface of Rift Valley fever virus. *Cell Rep.* 25, 3750–3758.e4.
- Alonso, D.O., Pérez-Sautu, U., Bellomo, C.M., Prieto, K., Iglesias, A., Coelho, R., Periolo, N., Domenech, I., Talmon, G., Hansen, R., et al. (2020). Person-to-person transmission of Andes virus in hantavirus pulmonary syndrome, Argentina, 2014. *Emerg. Infect. Dis.* 26, 756–759.
- Alvarado, G., and Crowe, J.E., Jr. (2016). Development of human monoclonal antibodies against respiratory syncytial virus using a high efficiency human hybridoma technique. *Methods Mol. Biol.* 1442, 63–76.
- Arikawa, J., Schmaljohn, A.L., Dalrymple, J.M., and Schmaljohn, C.S. (1989). Characterization of Hantaan virus envelope glycoprotein antigenic determinants defined by monoclonal antibodies. *J. Gen. Virol.* 70, 615–624.
- Arvin, A.M., Fink, K., Schmid, M.A., Cathcart, A., Spreafico, R., Havenar-Daughton, C., Lanzavecchia, A., Corti, D., and Virgin, H.W. (2020). A perspective on potential antibody-dependent enhancement of SARS-CoV-2. *Nature* 584, 353–363.
- Avsic-Zupanc, T., Xiao, S.Y., Stojanovic, R., Gligic, A., van der Groen, G., and LeDuc, J.W. (1992). Characterization of Dobrava virus: a Hantavirus from Slovenia, Yugoslavia. *J. Med. Virol.* 38, 132–137.
- Bangaru, S., Lang, S., Schotsaert, M., Vanderven, H.A., Zhu, X., Kose, N., Bombardi, R., Finn, J.A., Kent, S.J., Gilchuk, P., et al. (2019). A site of vulnerability on the influenza virus hemagglutinin head domain trimer interface. *Cell* 177, 1136–1152.e18.
- Bharadwaj, M., Nofchissey, R., Goade, D., Koster, F., and Hjelle, B. (2000). Humoral immune responses in the hantavirus cardiopulmonary syndrome. *J. Infect. Dis.* 182, 43–48.
- Bignon, E.A., Albornoz, A., Guardado-Calvo, P., Rey, F.A., and Tischler, N.D. (2019). Molecular organization and dynamics of the fusion protein Gc at the hantavirus surface. *eLife* 8, e46028.
- Botten, J., Mirowsky, K., Kusewitt, D., Bharadwaj, M., Yee, J., Ricci, R., Feddersen, R.M., and Hjelle, B. (2000). Experimental infection model for Sin Nombre hantavirus in the deer mouse (*Peromyscus maniculatus*). *Proc. Natl. Acad. Sci. USA* 97, 10578–10583.
- Boudreau, E.F., Joselyn, M., Ullman, D., Fisher, D., Dalrymple, L., Sellers-Myers, K., Loudon, P., Rusnak, J., Rivard, R., Schmaljohn, C., and Hooper, J.W. (2012). A Phase 1 clinical trial of Hantaan virus and Puumala virus M-segment DNA vaccines for hemorrhagic fever with renal syndrome. *Vaccine* 30, 1951–1958.
- Brocato, R.L., Joselyn, M.J., Wahl-Jensen, V., Schmaljohn, C.S., and Hooper, J.W. (2013). Construction and nonclinical testing of a Puumala virus synthetic M gene-based DNA vaccine. *Clin. Vaccine Immunol.* 20, 218–226.
- Brochet, X., Lefranc, M.P., and Giudicelli, V. (2008). IMGT/V-QUEST: the highly customized and integrated system for IG and TR standardized V-J and V-D-J sequence analysis. *Nucleic Acids Res.* 36, W503–W508.
- Chu, Y.K., Jennings, G., Schmaljohn, A., Eligh, F., Hjelle, B., Lee, H.W., Jenison, S., Ksiazek, T., Peters, C.J., Rollin, P., et al. (1995). Cross-neutralization of hantaviruses with immune sera from experimentally infected animals and from hemorrhagic fever with renal syndrome and hantavirus pulmonary syndrome patients. *J. Infect. Dis.* 172, 1581–1584.
- Corti, D., Voss, J., Gamblin, S.J., Codoni, G., Macagno, A., Jarrossay, D., Vachieri, S.G., Pinna, D., Minola, A., Vanzetta, F., et al. (2011). A neutralizing antibody selected from plasma cells that binds to group 1 and group 2 influenza A hemagglutinins. *Science* 333, 850–856.
- Custer, D.M., Thompson, E., Schmaljohn, C.S., Ksiazek, T.G., and Hooper, J.W. (2003). Active and passive vaccination against hantavirus pulmonary syndrome with Andes virus M genome segment-based DNA vaccine. *J. Virol.* 77, 9894–9905.
- Duehr, J., McMahon, M., Williamson, B., Amanat, F., Durbin, A., Hawman, D.W., Noack, D., Uhl, S., Tan, G.S., Feldmann, H., and Krammer, F. (2020). Neutralizing monoclonal antibodies against the Gn and the Gc of the Andes Virus glycoprotein spike complex protect from virus challenge in a preclinical hamster model. *MBio*. <https://doi.org/10.1128/mBio.00028-20>.
- Engdahl, T.B., and Crowe, J.E., Jr. (2020). Humoral immunity to hantavirus infection. *MSphere* 5. <https://doi.org/10.1128/mSphere.00482-20>.
- Fibriansah, G., Ibarra, K.D., Ng, T.S., Smith, S.A., Tan, J.L., Lim, X.N., Ooi, J.S., Kostyuchenko, V.A., Wang, J., de Silva, A.M., et al. (2015). Cryo-EM structure of an antibody that neutralizes dengue virus type 2 by locking E protein dimers. *Science* 349, 88–91.
- Flyak, A.I., Kuzmina, N., Murin, C.D., Bryan, C., Davidson, E., Gilchuk, P., Gulka, C.P., Ilynykh, P.A., Shen, X., Huang, K., et al. (2018). Broadly neutralizing antibodies from human survivors target a conserved site in the Ebola virus glycoprotein HR2-MPER region. *Nat. Microbiol.* 3, 670–677.
- Fox, J.M., Long, F., Edeling, M.A., Lin, H., van Duij-Richter, M.K.S., Fong, R.H., Kahle, K.M., Smit, J.M., Jin, J., Simmons, G., et al. (2015). Broadly neutralizing alphavirus antibodies bind an epitope on E2 and inhibit entry and egress. *Cell* 163, 1095–1107.
- Garrido, J.L., Prescott, J., Calvo, M., Bravo, F., Alvarez, R., Salas, A., Riquelme, R., Rioseco, M.L., Williamson, B.N., Haddock, E., et al. (2018). Two recombinant human monoclonal antibodies that protect against lethal Andes hantavirus infection in vivo. *Sci. Transl. Med.* 10, eaat6420.
- Gavrilovskaya, I.N., Shepley, M., Shaw, R., Ginsberg, M.H., and Mackow, E.R. (1998). beta3 integrins mediate the cellular entry of hantaviruses that cause respiratory failure. *Proc. Natl. Acad. Sci. USA* 95, 7074–7079.
- Gavrilovskaya, I.N., Brown, E.J., Ginsberg, M.H., and Mackow, E.R. (1999). Cellular entry of hantaviruses which cause hemorrhagic fever with renal syndrome is mediated by beta3 integrins. *J. Virol.* 73, 3951–3959.
- Gavrilovskaya, I.N., Gorbunova, E.E., and Mackow, E.R. (2010). Pathogenic hantaviruses direct the adherence of quiescent platelets to infected endothelial cells. *J. Virol.* 84, 4832–4839.
- Giudicelli, V., Brochet, X., and Lefranc, M.P. (2011). IMGT/V-QUEST: IMGT standardized analysis of the immunoglobulin (IG) and T cell receptor (TR) nucleotide sequences. *Cold Spring Harb. Protoc.* 2011, 695–715.
- Guardado-Calvo, P., Bignon, E.A., Stettner, E., Jeffers, S.A., Pérez-Vargas, J., Pehau-Arnaudet, G., Tortorici, M.A., Jestin, J.L., England, P., Tischler, N.D., and Rey, F.A. (2016). Mechanistic insight into bunyavirus-induced membrane fusion from structure-function analyses of the hantavirus envelope glycoprotein Gc. *PLoS Pathog.* 12, e1005813.
- Heiskanen, T., Lundkvist, A., Soliymani, R., Koivunen, E., Vaheri, A., and Lankinen, H. (1999). Phage-displayed peptides mimicking the discontinuous neutralization sites of puumala Hantavirus envelope glycoproteins. *Virology* 262, 321–332.

- Higa, M.M., Petersen, J., Hooper, J., and Doms, R.W. (2012). Efficient production of Hantaan and Puumala pseudovirions for viral tropism and neutralization studies. *Virology* 423, 134–142.
- Hooper, J.W., Custer, D.M., Thompson, E., and Schmaljohn, C.S. (2001a). DNA vaccination with the Hantaan virus M gene protects hamsters against three of four HFRS hantaviruses and elicits a high-titer neutralizing antibody response in rhesus monkeys. *J. Virol.* 75, 8469–8477.
- Hooper, J.W., Larsen, T., Custer, D.M., and Schmaljohn, C.S. (2001b). A lethal disease model for hantavirus pulmonary syndrome. *Virology* 289, 6–14.
- Hooper, J.W., Custer, D.M., Smith, J., and Wahl-Jensen, V. (2006). Hantaan/Andes virus DNA vaccine elicits a broadly cross-reactive neutralizing antibody response in nonhuman primates. *Virology* 347, 208–216.
- Hooper, J.W., Ferro, A.M., and Wahl-Jensen, V. (2008). Immune serum produced by DNA vaccination protects hamsters against lethal respiratory challenge with Andes virus. *J. Virol.* 82, 1332–1338.
- Hooper, J.W., Josley, M., Ballantyne, J., and Brocato, R. (2013). A novel Sin Nombre virus DNA vaccine and its inclusion in a candidate pan-hantavirus vaccine against hantavirus pulmonary syndrome (HPS) and hemorrhagic fever with renal syndrome (HFRS). *Vaccine* 31, 4314–4321.
- Hooper, J.W., Brocato, R.L., Kwiłas, S.A., Hammerbeck, C.D., Josley, M.D., Royals, M., Ballantyne, J., Wu, H., Jiao, J.A., Matsushita, H., and Sullivan, E.J. (2014a). DNA vaccine-derived human IgG produced in transchromosomal bovines protect in lethal models of hantavirus pulmonary syndrome. *Sci. Transl. Med.* 6, 264ra162.
- Hooper, J.W., Moon, J.E., Paolino, K.M., Newcomer, R., McLain, D.E., Josley, M., Hannaman, D., and Schmaljohn, C. (2014b). A Phase 1 clinical trial of Hantaan virus and Puumala virus M-segment DNA vaccines for hemorrhagic fever with renal syndrome delivered by intramuscular electroporation. *Clin. Microbiol. Infect.* 20 (Suppl 5), 110–117.
- Huiskonen, J.T., Hepojoki, J., Laurimäki, P., Vaheri, A., Lankinen, H., Butcher, S.J., and Grünewald, K. (2010). Electron cryotomography of Tula hantavirus suggests a unique assembly paradigm for enveloped viruses. *J. Virol.* 84, 4889–4897.
- Jangra, R.K., Herbert, A.S., Li, R., Jae, L.T., Kleinfelter, L.M., Slough, M.M., Barker, S.L., Guardado-Calvo, P., Román-Sosa, G., Dieterle, M.E., et al. (2018). Protocadherin-1 is essential for cell entry by New World hantaviruses. *Nature* 563, 559–563.
- Katzelnick, L.C., Gresh, L., Halloran, M.E., Mercado, J.C., Kuan, G., Gordon, A., Balmaseda, A., and Harris, E. (2017). Antibody-dependent enhancement of severe dengue disease in humans. *Science* 358, 929–932.
- Kitamura, T., Morita, C., Komatsu, T., Sugiyama, K., Arikawa, J., Shiga, S., Takeda, H., Akao, Y., Imaizumi, K., Oya, A., et al. (1983). Isolation of virus causing hemorrhagic fever with renal syndrome (HFRS) through a cell culture system. *Jpn. J. Med. Sci. Biol.* 36, 17–25.
- Koch, J., Liang, M., Queitsch, I., Kraus, A.A., and Bautz, E.K. (2003). Human recombinant neutralizing antibodies against hantaan virus G2 protein. *Virology* 308, 64–73.
- Kruger, D.H., Figueiredo, L.T., Song, J.W., and Kiemba, B. (2015). Hantaviruses—globally emerging pathogens. *J. Clin. Virol.* 64, 128–136.
- Lee, H.W., Lee, P.W., and Johnson, K.M. (1978). Isolation of the etiologic agent of Korean Hemorrhagic fever. *J. Infect. Dis.* 137, 298–308.
- Li, S., Rissanen, I., Zeltina, A., Hepojoki, J., Raghwani, J., Harlos, K., Pybus, O.G., Huiskonen, J.T., and Bowden, T.A. (2016). A molecular-level account of the antigenic hantaviral surface. *Cell Rep.* 15, 959–967.
- Lundkvist, A., Hukic, M., Hörling, J., Gilljam, M., Nichol, S., and Niklasson, B. (1997). Puumala and Dobrava viruses cause hemorrhagic fever with renal syndrome in Bosnia-Herzegovina: evidence of highly cross-neutralizing antibody responses in early patient sera. *J. Med. Virol.* 53, 51–59.
- Martinez, V.P., Bellomo, C., San Juan, J., Pinna, D., Forlenza, R., Elder, M., and Padula, P.J. (2005). Person-to-person transmission of Andes virus. *Emerg. Infect. Dis.* 11, 1848–1853.
- Martínez, V.P., Di Paola, N., Alonso, D.O., Pérez-Sautu, U., Bellomo, C.M., Iglesias, A.A., Coelho, R.M., López, B., Periolo, N., Larson, P.A., et al. (2020). “Super-Spreaders” and Person-to-Person Transmission of Andes Virus in Argentina. *N. Engl. J. Med.* 383, 2230–2241.
- Matute-Bello, G., Frevert, C.W., and Martin, T.R. (2008). Animal models of acute lung injury. *Am. J. Physiol. Lung Cell. Mol. Physiol.* 295, L379–L399.
- McCoy, L.E., Falkowska, E., Doores, K.J., Le, K., Sok, D., van Gils, M.J., Euler, Z., Burger, J.A., Seaman, M.S., Sanders, R.W., et al. (2015). Incomplete neutralization and deviation from sigmoidal neutralization curves for HIV broadly neutralizing monoclonal antibodies. *PLoS Pathog.* 11, e1005110.
- Morens, D.M., and Fauci, A.S. (2020). Emerging pandemic diseases: how we got to COVID-19. *Cell* 182, 1077–1092.
- Parvate, A., Williams, E.P., Taylor, M.K., Chu, Y.K., Lanman, J., Saphire, E.O., and Jonsson, C.B. (2019). Diverse morphology and structural features of Old and New World hantaviruses. *Viruses* 11, 862.
- Perley, C.C., Brocato, R.L., Wu, H., Bausch, C., Karmali, P.P., Vega, J.B., Cohen, M.V., Somerville, B., Kwiłas, S.A., Principe, L.M., et al. (2020). Anti-HFRS human IgG produced in transchromosomal bovines has potent hantavirus neutralizing activity and is protective in animal models. *Front. Microbiol.* 11, 832.
- Plyusnin, A., Vapalahti, O., and Vaheri, A. (1996). Hantaviruses: genome structure, expression and evolution. *J. Gen. Virol.* 77, 2677–2687.
- Powell, L.A., Fox, J.M., Kose, N., Kim, A.S., Majedi, M., Bombardi, R., Carnahan, R.H., Slaughter, J.C., Morrison, T.E., Diamond, M.S., and Crowe, J.E., Jr. (2020a). Human monoclonal antibodies against Ross River virus target epitopes within the E2 protein and protect against disease. *PLoS Pathog.* 16, e1008517.
- Powell, L.A., Miller, A., Fox, J.M., Kose, N., Klose, T., Kim, A.S., Bombardi, R., Tennekoon, R.N., Dharshan de Silva, A., Carnahan, R.H., et al. (2020b). Human mAbs broadly protect against arthritogenic alphaviruses by recognizing conserved elements of the Mxra8 receptor-binding site. *Cell Host Microbe* 28, 699–711.e7.
- Prist, P.R., Uriarte, M., Tambosi, L.R., Prado, A., Pardini, R., D Andrea, P.S., and Metzger, J.P. (2016). Landscape, environmental and social predictors of hantavirus risk in São Paulo, Brazil. *PLoS ONE* 11, e0163459.
- Ray, N., Whidby, J., Stewart, S., Hooper, J.W., and Bertolotti-Ciarlet, A. (2010). Study of Andes virus entry and neutralization using a pseudovirion system. *J. Virol. Methods* 163, 416–423.
- Rissanen, I., Stass, R., Krumm, S.A., Seow, J., Hulswit, R.J., Paesen, G.C., Hepojoki, J., Vapalahti, O., Lundkvist, Å., Reynard, O., et al. (2020). Molecular rationale for antibody-mediated targeting of the hantavirus fusion glycoprotein. *eLife* 9, e58242.
- Schmaljohn, C.S., Spik, K.W., and Hooper, J.W. (2014). DNA vaccines for HFRS: laboratory and clinical studies. *Virus Res.* 187, 91–96.
- Schnell, M.J., Buonocore, L., Kretzschmar, E., Johnson, E., and Rose, J.K. (1996). Foreign glycoproteins expressed from recombinant vesicular stomatitis viruses are incorporated efficiently into virus particles. *Proc. Natl. Acad. Sci. USA* 93, 11359–11365.
- Serris, A., Stass, R., Bignon, E.A., Muena, N.A., Manuguerra, J.C., Jangra, R.K., Li, S., Chandran, K., Tischler, N.D., Huiskonen, J.T., et al. (2020). The hantavirus surface glycoprotein lattice and its fusion control mechanism. *Cell* 183, 442–456.e16.
- Smith, S.A., and Crowe, J.E., Jr. (2015). Use of human hybridoma technology to isolate human monoclonal antibodies. *Microbiol. Spectr.* 3, AID-0027-2014.
- Smith, S.A., Zhou, Y., Olivarez, N.P., Broadwater, A.H., de Silva, A.M., and Crowe, J.E., Jr. (2012). Persistence of circulating memory B cell clones with potential for dengue virus disease enhancement for decades following infection. *J. Virol.* 86, 2665–2675.
- Tischler, N.D., Galeno, H., Rosembatt, M., and Valenzuela, P.D. (2005). Human and rodent humoral immune responses to Andes virus structural proteins. *Virology* 334, 319–326.
- Tkachenko, E.A., Bashirksev, V.N., van der Groen, G., Dzagurova, T.K., Ivanov, A.P., and Ryltseva, E.V. (1984). Isolation in Vero-E6 cells of Hanta virus

- from Clethrionomys glareolus captured in the Bashkiria area of the U.S.S.R. *Ann. Soc. Belg. Med. Trop.* 64, 425–426.
- Turchaninova, M.A., Davydov, A., Britanova, O.V., Shugay, M., Bikos, V., Egorov, E.S., Kirgizova, V.I., Merzlyak, E.M., Staroverov, D.B., Bolotin, D.A., et al. (2016). High-quality full-length immunoglobulin profiling with unique molecular barcoding. *Nat. Protoc.* 11, 1599–1616.
- Wahl-Jensen, V., Chapman, J., Asher, L., Fisher, R., Zimmerman, M., Larsen, T., and Hooper, J.W. (2007). Temporal analysis of Andes virus and Sin Nombre virus infections of Syrian hamsters. *J. Virol.* 81, 7449–7462.
- Wang, M., Pennock, D.G., Spik, K.W., and Schmaljohn, C.S. (1993). Epitope mapping studies with neutralizing and non-neutralizing monoclonal antibodies to the G1 and G2 envelope glycoproteins of Hantaan virus. *Virology* 197, 757–766.
- Webb, N.E., Montefiori, D.C., and Lee, B. (2015). Dose-response curve slope helps predict therapeutic potency and breadth of HIV broadly neutralizing antibodies. *Nat. Commun.* 6, 8443.
- Wee, A.Z., Nyakatura, E.K., Herbert, A.S., Howell, K.A., Holtsberg, F.W., Bakken, R.R., Mittler, E., Christin, J.R., Shulenin, S., Jangra, R.K., et al. (2016). A “Trojan horse” bispecific-antibody strategy for broad protection against ebolaviruses. *Science* 354, 350–354.
- Wee, A.Z., Wrapp, D., Herbert, A.S., Maurer, D.P., Haslwanter, D., Sakharakar, M., Jangra, R.K., Dieterle, M.E., Lilov, A., Huang, D., et al. (2020). Broad neutralization of SARS-related viruses by human monoclonal antibodies. *Science* 369, 731–736.
- Whitt, M.A. (2010). Generation of VSV pseudotypes using recombinant ΔG-VSV for studies on virus entry, identification of entry inhibitors, and immune responses to vaccines. *J. Virol. Methods* 169, 365–374.
- Willensky, S., Bar-Rogovsky, H., Bignon, E.A., Tischler, N.D., Modis, Y., and Dessaub, M. (2016). Crystal structure of glycoprotein C from a hantavirus in the post-fusion conformation. *PLoS Pathog.* 12, e1005948.
- Yao, J.S., Kariwa, H., Takashima, I., Arikawa, J., and Hashimoto, N. (1992). Antibody-dependent enhancement of hantavirus infection in macrophage cell lines. *Arch. Virol.* 122, 107–118.
- Yu, X., McGraw, P.A., House, F.S., and Crowe, J.E., Jr. (2008). An optimized electrofusion-based protocol for generating virus-specific human monoclonal antibodies. *J. Immunol. Methods* 336, 142–151.

STAR★METHODS

KEY RESOURCES TABLE

REAGENT or RESOURCE	SOURCE	IDENTIFIER
Antibodies		
DENV 2D22	(Smith et al., 2012)	N/A
rDENV-2D22 IgG (recombinant expiCHO-produced IgG1)	(Fibriansah et al., 2015)	N/A
SNV-3 (hybridoma cell produced IgG1)	This paper	N/A
SNV-21 (hybridoma cell produced IgG1)	This paper	N/A
SNV-24 (hybridoma cell produced IgG1)	This paper	N/A
rSNV-24 (recombinant CHO cell produced IgG1)	This paper	N/A
SNV-25 (hybridoma cell produced IgG1)	This paper	N/A
SNV-27 (hybridoma cell produced IgG1)	This paper	N/A
SNV-30 (hybridoma cell produced IgG1)	This paper	N/A
rSNV-30 (recombinant CHO cell produced IgG1)	This paper	N/A
SNV-32 (hybridoma cell produced IgG1)	This paper	N/A
SNV-36 (hybridoma cell produced IgG1)	This paper	N/A
SNV-39 (hybridoma cell produced IgG1)	This paper	N/A
SNV-42 (hybridoma cell produced IgG1)	This paper	N/A
SNV-45 (hybridoma cell produced IgG1)	This paper	N/A
SNV-50 (hybridoma cell produced IgG1)	This paper	N/A
SNV-53 (hybridoma cell produced IgG1)	This paper	N/A
rSNV-53 (recombinant CHO cell produced IgG1)	This paper	N/A
SNV-56 (hybridoma cell produced IgG1)	This paper	N/A
SNV-57 (hybridoma cell produced IgG2)	This paper	N/A
SNV-62 (hybridoma cell produced IgG1)	This paper	N/A
SNV-65 (hybridoma cell produced IgG1)	This paper	N/A
SNV-66 (hybridoma cell produced IgG1)	This paper	N/A
SNV-67 (hybridoma cell produced IgG1)	This paper	N/A
SNV-68 (hybridoma cell produced IgG1)	This paper	N/A
ANDV-2 (hybridoma cell produced IgG1)	This paper	N/A
ANDV-3 (hybridoma cell produced IgG1)	This paper	N/A
ANDV-4 (hybridoma cell produced IgG1)	This paper	N/A
ANDV-5 (hybridoma cell produced IgG1)	This paper	N/A
rANDV-5 (recombinant CHO cell produced IgG1)	This paper	N/A
ANDV-11 (hybridoma cell produced IgG1)	This paper	N/A
ANDV-12 (hybridoma cell produced IgG1)	This paper	N/A
ANDV-22 (hybridoma cell produced IgG1)	This paper	N/A
ANDV-23 (hybridoma cell produced IgG1)	This paper	N/A
ANDV-34 (hybridoma cell produced IgG1)	This paper	N/A
ANDV-38 (hybridoma cell produced IgG1)	This paper	N/A
ANDV-42 (hybridoma cell produced IgG1)	This paper	N/A
ANDV-43 (hybridoma cell produced IgG1)	This paper	N/A
ANDV-44 (hybridoma cell produced IgG1)	This paper	N/A

(Continued on next page)

Continued

REAGENT or RESOURCE	SOURCE	IDENTIFIER
rANDV-44 (recombinant CH cell produced IgG1)	This paper	N/A
ANDV-54 (hybridoma cell produced IgG1)	This paper	N/A
ANDV-59 (hybridoma cell produced IgG1)	This paper	N/A
ANDV-69 (hybridoma cell produced IgG1)	This paper	N/A
Goat Anti-Human IgG-PE	Southern Biotech	Cat# 2040-09; RRID:AB_2795648
Goat Anti-Human IgG (Fc)	Meridian Life Sciences	Cat# W99008A; RRID:AB_205090
KPL affinity Goat anti Human IgG (γ)	SeraCare	Cat# 5220-0456
AEC Substrate system	Enquire BioReagents	Cat# QS-9
Goat anti-Human IgG (H+L) Cross-Adsorbed Secondary Antibody, Alexa Fluor 568	Thermo Fisher Scientific	Cat# A-21090
Anti-Sin Nombre Virus Glycoprotein 1 antibody produced in rabbit	Sigma-Aldrich	Cat# SAB3501093-100UG
Anti-Sin Nombre Virus Glycoprotein 2 antibody produced in rabbit	Sigma-Aldrich	Cat# SAB3501094-100UG
anti-SNV rabbit serum	Christina Spiropoulou, CDC	unpublished
Anti-HTNV rabbit serum (DNA vaccine-derived) Lot SK091615	Hooper, USAMRIID	unpublished
Anti-PUUV rabbit serum (DNA vaccine-derived) Lot JH091514	Hooper, USAMRIID	unpublished
Anti-SEOV rabbit serum (DNA vaccine-derived) Lot MC120516	Hooper, USAMRIID	unpublished
Anti-DOBV rabbit serum (DNA vaccine-derived) Lot MC122816	Hooper, USAMRIID	unpublished
HRP-labeled mAb-H13-3d7 G2 Life Tech/C29B5B/120432A	Hooper, USAMRIID	unpublished
Bacterial and virus strains		
Andes virus strain Chile-9717869 (Chile R123)	UTMB Arbovirus Reference Collection	N/A
Sin Nombre virus strain SN77734	UTMB Arbovirus Reference Collection	N/A
Hantaan virus strain 76-118	USAMRIID Collection	Lee et al., 1978
Dobrava virus strain Dobrava	USAMRIID Collection	Avsic-Zupanc et al., 1992
Puumala virus strain K27	USAMRIID Collection	Tkachenko et al., 1984
Seoul virus strain SR-11	USAMRIID Collection	Kitamura et al., 1983
pVSV/SNV	This paper	N/A
pVSV/ANDV	This paper	N/A
pVSV/HTNV	This paper	N/A
pVSV/SEOV	This paper	N/A
pVSV/PUUV	This paper	N/A
pVSV/DOBV	This paper	N/A
Pseudotyped Δ G-GFP (G \star Δ G-GFP) rVSV	Kerafast	Cat# EH1019-PM
Biological samples		
PBMCs from SNV-immune donor	This paper	Vanderbilt Vaccine Center Biorepository ID #1513
PBMCs from SNV-immune donor (laboratory confirmed infection in 2010)	This paper	Vanderbilt Vaccine Center Biorepository ID #1487
PBMCs from SNV-immune donor (laboratory confirmed infection in 2017)	This paper	Vanderbilt Vaccine Center Biorepository ID #1486

(Continued on next page)

Continued

REAGENT or RESOURCE	SOURCE	IDENTIFIER
PBMCs from ANDV-immune donor	This paper	Vanderbilt Vaccine Center Biorepository ID #1685
Chemicals, peptides, and recombinant proteins		
Cyclosporin A (CSA)	Sigma-Aldrich	Cat# C1832
CpG	Sigma-Aldrich	Cat# C3742-25MG
Chk2 inhibitor	Sigma-Aldrich	Cat# C3742
ClonaCell-HY Medium A	STEMCELL Technologies	Cat# 3801
ClonalCell-HY Medium E	STEMCELL Technologies	Cat# 3805
384-well plate	Nunc	Cat# 164688
384-well plate (non-treated)	Thermo Fisher Nunc	Cat# 262203
96-well U-bottom plate	Thermo Fisher Scientific	Cat# 163320
96-well flat bottom plate	Thermo Fisher Scientific	Cat# 167008
96-well plate	Falcon	Cat# 353072
96-well plate, μCLEAR	Greiner Bio-one	Cat# 655090
96-well plate, v-bottom	Corning	Cat# 3894
ExpiFectamine 293 Transfection Kit	Thermo Fisher Scientific	Cat# A14525
Ouabain	Sigma-Aldrich	Cat# O3125
Hypoxanthine	Sigma-Aldrich	Cat# H0137
HAT	Sigma-Aldrich	Cat# H0262
G-rex	Wilson Wolf	Cat# 80240M
Hybridoma Serum Free Media	GIBCO	Cat# 12045
T-75 flasks	Falcon	Cat# 353136
HiTrap MabSelectSure	Cytiva	Cat# 11003494
Freestyle F17 Expression Medium	GIBCO	Cat# A13835-01
ExpiCHO Expression Medium	Thermo Fisher Scientific	Cat# A2910001
10% Pluronic F-68	GIBCO	Cat# 240400-32
L-Glutamine	GIBCO	Cat# 25030-081
Opti-MEM 1 Reduced Serum Medium	GIBCO	Cat# 31985088
Fetal Bovine Serum, ultra-low IgG	Thermo Fisher Scientific	Cat# 16250078
Vascular Cell Basal Medium	ATCC	Cat# PCS-100-030
Endothelial Cell Growth Kit-VEGF	ATCC	Cat# PCS-100-041
Trypsin EDTA (0.25%), Phenol Red	Thermo Fisher Scientific	Cat# 25200114
DMEM, high glucose	Thermo Fisher Scientific	Cat# 11965118
FBS, heat inactivated	Thermo Fisher Scientific	Cat# A3840102
96 well clear V-bottom plate	Corning	Cat# 3894
D-PBS	Corning	Cat# 21031CM
Lipofectamine 2000	Thermo Fisher Scientific	Cat# 11668027
Lipofectamine 3000 Transfection Reagent	Thermo Fisher Scientific	Cat# L3000015
DAPI (4',6-Diamidino-2-Phenylindole, Dihydrochloride)	Thermo Fisher Scientific	Cat# D1306
Histopaque(R)-1077, sterile-filtered, density: 1.077 g/mL	Sigma-Aldrich	Cat# 10771-500ML
AP substrate	Sigma-Aldrich	Cat# S0942-200AAB
Alexa Fluor 647 NHS Ester (Succinimidyl Ester)	Thermo Fisher Scientific	Cat# A37573
Recombinant DNA		

(Continued on next page)

Continued

REAGENT or RESOURCE	SOURCE	IDENTIFIER
pWRG/SN-M(opt)	Jay Hooper, USAMRIID	Hooper et al., 2013
pWRG/AND-M(opt2)	Jay Hooper, USAMRIID	(Hooper et al., 2014a)
pWRG/PUU-M(s2)	Jay Hooper, USAMRIID	Brocato et al., 2013
pWRG/DOB-M(opt)	Jay Hooper, USAMRIID	Perley et al., 2020
pWRG/HTN-M(co)	Jay Hooper, USAMRIID	(Schmaljohn et al., 2014)
pWRG/SEO-M(opt2)	Jay Hooper, USAMRIID	Perley et al., 2020
pCAGGS-G-Kan plasmid	Kerafast	Cat# EH1017
pTwist_SNV-24_mCisL	This paper	Twist Biosciences Inc.
pTwist_SNV-30_mCisK	This paper	Twist Biosciences Inc.
pTwist_SNV-53_mCisL	This paper	Twist Biosciences Inc.
pTwist_ANDV-44_mCisK	This paper	Twist Biosciences Inc.
pTwist_ANDV-5_mCisK	This paper	Twist Biosciences Inc.
pcDNA3.1+_sEC1	Jangra et al., 2018; GenBank: NM_002587	GenScript Biotech
pcDNA3.1+_ANDV_Gc_ectodomain	This paper; GenBank: QNQ18210.1	GenScript Biotech
pcDNA3.1+_ANDV_Gn_full length	This paper; GenBank: QNQ18210.1	GenScript Biotech
pcDNA3.1+_SNV_Gc_ectodomain	This paper; GenBank: KF537002.1	GenScript Biotech
pCAGGS_SNV_Gn_full length	This paper; : GenBank: NP_941974	GenScript Biotech
Critical commercial assays		
Universal Mycoplasma Detection Kit	ATCC	Cat# 30-1012K
Pierce BCA Protein Assay Kit	Thermo Fisher Scientific	Cat# 23225
Experimental models: cell lines		
Monkey: B95.8	ATCC	Cat# VR-1492 (discontinued); RRID:CVCL_1953
Human: Expi293F	Thermo Fisher Scientific	Cat# A14527; RRID:CVCL_D615
Hamster: ExpiCHO	Thermo Fisher Scientific	Cat# A29127; RRID:CVCL_5J31
Hamster: BHK-21 (WI-2)	Kerafast	Cat# EH1011; RRID:CVCL_HB78
Monkey: Vero E6	ATCC	Cat# CCL-81; RRID:CVCL_0059
Monkey: Vero C1008	ATCC	Cat# CRL-1586; RRID:CVCL_0574
Human: Primary Umbilical Vein Endothelial Cells; Normal, Pooled (HUVEC)	ATCC	Cat# PCS-100-013
Mouse-human HMMA 2.5 myeloma cell line	Dr. L. Cavacini	N/A
Software and algorithms		
Prism	GraphPad Software, Inc.	v8
FlowJo	Tree Star Inc.	v10
BioSpot 5.1 software	CTL	N/A
MetaXpress	Molecular Devices	N/A
iQue® Forecyt® Software	Sartorius	N/A
ImMunoGeneTics (IMGT) database	(Brochet et al., 2008); Giudicelli et al., 2011	N/A
Other		
Sony SH800S Cell Sorter	Sony	N/A
ÄKTA pure chromatography system	GE Healthcare	N/A
HiTrap Protein G High Performance	GE Healthcare	Cat# 28-9075-48
ImmunoSpot plate reader	CTL	N/A
Intellicyt iQue Screener Plus IntelliCyt®	Sartorius	N/A
iQue Screener PLUS		
ImageXpress Micro XL	Molecular Devices	N/A
BioStack 3 Microplate Stacker	BioTek	Cat# BIOSTACK3WR
EL406 Washer Dispenser	BioTek	Cat# 406SUB3
PacBio Sequel System	Pacific Biosciences	N/A

RESOURCE AVAILABILITY

Lead contact

Further information and requests for resources and reagents should be directed to and will be fulfilled by the lead contact, James E. Crowe, Jr. (james.crowe@vumc.org).

Materials availability

Materials described in this paper are available for distribution for nonprofit use using templated documents from Association of University Technology Managers “Toolkit MTAs,” available at: <https://autm.net/surveys-and-tools/agreements/material-transfer-agreements/mta-toolkit>.

Data and code availability

All data needed to evaluate the conclusions in the paper are present in the paper or the Supplemental Information. The ANDV or SNV antibodies in this study are available by Material Transfer Agreement with Vanderbilt University Medical Center. Original/source data for all figures in the paper is available at Mendeley Data <https://doi.org/10.17632/36yhsg4b36.1>.

EXPERIMENTAL MODEL AND SUBJECT DETAILS

Cell lines

All cell lines were tested for mycoplasma monthly, and all samples were negative. Expi293F cells (ATCC, female) were cultured in suspension at 37°C in 8% CO₂ shaking at 125 RPM in Freestyle F17 Expression Medium (GIBCO) supplemented with 10% Pluronic F-68 and 200 mM of L-glutamine. ExpiCHO cells (ATCC, female) were cultured in suspension at 37°C in 8.0% CO₂ shaking at 125 RPM in ExpiCHO Expression Medium (Thermo Fisher). B95.8 cells (ATCC® CRL-1612, female) producing Epstein-Barr virus and the non-secreting myeloma HMMA2.5 heteromyeloma cell line (kindly provided by Lisa Cavacini, female human and female mice elements) used as the fusion partner for human B cell hybridoma formation each were cultured at 37°C in 8% CO₂ in ClonaCell-HY medium A. BHK-21(WI-2) cell lines (Kerafast, golden Syrian hamster, sex unspecified) and Vero E6 cell lines (ATCC, CCL-81, African green monkey, sex unspecified) were cultured at 37°C in 8% CO₂ in DMEM supplemented with 10% fetal bovine serum. PBMCs (obtained from leukofiltration filters, Nashville Red Cross, male) were irradiated and cryopreserved in Medium A containing 10% DMSO. Vero E6 cell lines (Vero C1008, ATCC CRL 1586, African green monkey, sex female) were maintained in Eagle's minimum essential medium with Earle's salts containing 10% fetal bovine serum (FBS), 10 mM HEPES (pH 7.4), 1 × penicillin-streptomycin, amphotericin B (0.5 µg/mL) and gentamicin sulfate (50 µg/mL) (cEMEM) at 37°C in 5% CO₂.

Human subjects

SNV-immune subject (Donor ID# 1486) was a 57-year-old male from Utah diagnosed with hantavirus infection on June 6, 2017. Peripheral blood was obtained from this subject in the U.S. on June 20, 2018 (1 year after infection). SNV-immune subject (Donor ID# 1487) was a 36-year-old female from Kansas diagnosed with hantavirus infection in December 2010. Peripheral blood was obtained from this subject in the U.S. on July 20, 2018 (8 years after infection). SNV-immune subject (Donor ID# 1513) was a 41-year-old male from Texas diagnosed with hantavirus infection on an unknown date. Peripheral blood was obtained from this subject in the U.S. on April 3, 2018. Written informed consent with approval from the Vanderbilt University Medical Center Institutional Review Board was given by all human subjects. Peripheral blood mononuclear cells (PBMCs) were isolated using density gradient centrifugation on Ficoll and were cryopreserved in liquid nitrogen until used in the experiments. ANDV-immune subject (donor ID# 1685) was diagnosed with hantavirus infection in December 2006. Peripheral blood was obtained from this subject on June 10, 2015 at the Universidad Del Desarrollo, Chile (9 years after infection). The studies were approved by the Institutional Review Boards of the Facultad de Medicina Clinica Alemana-Universidad Del Desarrollo and Vanderbilt University Medical Center. PBMCs were transferred to Vanderbilt using a liquid nitrogen dry shipper in 2015.

Viruses

Andes virus strain Chile-9717869 (Chile R123) and Sin Nombre virus strain SN77734 were obtained from the World Reference Center for Emerging Viruses and Arboviruses housed at UTMB. The SNV strain used was isolated previously from deer mice (*Peromyscus maniculatus*) (Botten et al., 2000). Hantaan virus strain 76-118 (Lee et al., 1978), PUUV strain K27 (Tkachenko et al., 1984), Dobrava virus strain Dobrava (Avsic-Zupanc et al., 1992), and Seoul virus strain SR-11 (Kitamura et al., 1983) were propagated in Vero E6 cells (Vero C1008, ATCC CRL 1586) in T-150 flasks and collected from infected-monolayer supernatants (between days 7 to 10). Cell debris was removed by low-speed centrifugation in a table-top centrifuge and virus stocks were stored at -60°C or colder until use.

Animal model

Eight-week-old female golden Syrian hamsters, strain HsdHan®:AURA, were used for testing of the protective efficacy. All animal experiments and procedures were carried out in accordance with the recommendations in the Guide for the Care and Use of Laboratory Animals of the National Institutes of Health. The protocols were approved by the Institutional Animal Care and Use Committee

at the University of Texas Medical Branch (protocol #1912091). Injections were performed under anesthesia induced by ketamine hydrochloride and xylazine, and all efforts were made to minimize animal suffering.

METHOD DETAILS

Generation of cell-surface expressed antigens

Plasmids containing a cDNA encoding the full-length M segment from various hantavirus species (pWRG/SN-M(opt) [Hooper et al., 2013], pWRG/AND-M(opt2) [Hooper et al., 2014a], pWRG/PUU-M(s2) [Brocato et al., 2013], pWRG/DOB-M(opt), pWRG/HTN-M(co) [Hooper et al., 2001a], and pWRG/SEO-M(opt2) [Hooper et al., 2001a]) were used to produce cell-surface displayed hantavirus antigens. Expi293F cells were cultured in Freestyle F17 expression medium (GIBCO) containing 10% Pluronic F-68 and 200 mM L-glutamine, and transiently transfected with plasmid DNA using the Expifectamine 293 transfection kit (Thermo Fisher). Expi293F cells were harvested 48 hours after transfection and cryopreserved for use in flow cytometry assays.

Screening and binding of NWH-reactive antibodies

A flow cytometric assay was used to screen for, and quantify binding of, NWH-reactive antibodies. Expi293F cells transfected with the full-length M segment as described above were thawed, strained through a 40 µm cell strainer, and plated into 96-well V-bottom plates at 30,000 cells/well in FACS buffer (2% ultra-low IgG FBS, 1 mM EDTA, D-PBS). Cells were incubated with purified mAb or cell supernatant for 1 hour at 4°C, washed twice with FACS buffer, and stained with a 1:1,000 solution of goat anti-human IgG antibodies conjugated to phycoerythrin (PE) (Southern Biotech) at 4°C for 30 minutes. Cells then were washed twice with FACS buffer and stained for 5 minutes at 4°C with 0.5 µg/mL of 4',6-diamidino-2-phenylindole (DAPI) (Thermo Fisher). PE and DAPI staining were measured with an iQue Screener Plus flow cytometer (Intelicyt) and quantified using the manufacturer's ForeCyt software. A value for percent PE-positive cells was determined by gating based on the relative fluorescence intensity of Expi293F cells stained only with secondary antibody.

Isolation of human hybridomas and purification of monoclonal antibodies

Peripheral blood mononuclear cells (PBMCs) were isolated from immune subject blood samples using Ficoll-Histopaque (Sigma-Aldrich) density gradient centrifugation and cryopreserved in the vapor phase of liquid nitrogen until use. PBMCs were thawed and 6 million cells were transformed with 4.5 mL of filtered supernatant containing Epstein-Barr virus (in the collected supernatant from cultured B95.8 cells) and plated in medium containing 2.5 µg/mL CpG (phosphorothioate-modified oligodeoxynucleotide ZOE-ZOEZZZZOEEZOEZ, Invitrogen), 10 µM Chk2 inhibitor (Sigma-Aldrich, Cat. No. C3742), and 10 µg/mL cyclosporine A (Sigma-Aldrich, Cat. No. C1832) and plated in a 384-well plate. After 7 days, lymphoblastoid cell lines (LCLs) were expanded on feeder layers containing irradiated PBMCs (obtained from leukofiltration filters, Nashville Red Cross) in 96-well plates. LCL supernatant was collected and screened in a flow cytometric assay using Expi293F-SNV-M cells, Expi293F-ANDV-M cells, or mock-transfected Expi293F cells. An anti-human IgG secondary conjugated PE antibody (Southern Biotech) was used for detection. Cell lines secreting NWH-reactive antibodies were identified by gating based on mock-transfected Expi293F cells. LCLs in antigen-reactive wells then were fused with HMMA2.5 cells by electrofusion to produce hybridomas and plated in medium containing 100 µM hypoxanthine, 0.4 µM aminopterin, 16 µM thymidine, and 7 µg/mL ouabain. Hybridomas were cultured for 3 weeks and then screened again in a flow cytometric binding assay using Expi293F-SNV-M or Expi293F-ANDV-M to identify cells secreting SNV and ANDV-reactive antibodies. Positive wells were single-cell sorted into 384-well plates on a SH800S Cell Sorter (Sony). Single cells then were incubated for 3–4 weeks and screened against Expi293F-SNV-M or Expi293F-ANDV-M cells by flow cytometry to identify positive clones. Hybridoma clones secreting antibodies that reacted with Expi293F-SNV-M or Expi293F-ANDV-M cells then were expanded to G-Rex 6-well plates (Wilson Wolf) and grown in Hybridoma Serum Free Medium (GIBCO) for 2–4 weeks. Supernatant was harvested from G-Rex plates and filtered with 0.45-µm pore size filter flasks. HiTrap MabSelectSure columns (Cytiva) then were used to affinity purify mAbs from hybridoma supernatant using an AKTA pure protein purification system (Cytiva).

Antibody gene sequence analysis

RNA was extracted and amplified from cloned hybridoma cell pellets based on a modified 5' Rapid Amplification of cDNA Ends (5' RACE) as previously described (Turchaninova et al., 2016). Prepped amplicon libraries were then sequenced using a Sequel Platform (Pacific Biosciences). Isotype and subclass was determined through sequence of constant regions Sequence analysis to determine the antibody gene segments, complementarity determining regions (CDRs), and % mutation from germline was performed using ImMunoGeneTics (IMGT) V-QUEST tool (Giudicelli et al., 2011). cDNAs encoding antibody genes for heavy and light chains were cloned into a vector expressing full-length IgG1 (Twist Biosciences). ExpiCHO cells were transiently transfected with plasmids encoding full-length IgG cDNAs. Supernatant was harvested from ExpiCHO cultures and filtered with 0.45-µm pore size filter flasks. HiTrap MabSelectSure columns (Cytiva) then were used to affinity purify mAbs from ExpiCHO supernatant using an AKTA pure protein purification system (Cytiva). Recombinant antibodies were used in animal studies described below.

Generation of pseudotyped VSVs

All pseudotyped viruses were generated based on a previously published protocol (Whitt, 2010) using plasmids pWRG/SN-M(opt), pWRG/AND-M(opt2), pWRG/PUU-M(s2), pWRG/DOB-M(opt), pWRG/HTN-M(co), pWRG/SEO-M(opt2), and pCAGGS-G-Kan (Kerafast, kindly provided by Dr. Michael A. Whitt). BHK-21(WI-2) cells were plated in a 6-well plate at a density of 100,000 cells/well. 24 hours later, cells were transfected with 10 µL of Lipofectamine 3000 and P300 reagent (Thermo Fisher) and 2.5 µg of plasmid DNA, and medium was removed and replaced with normal growth medium 4 hours later. 48 hours after transfection, cells were inoculated with G*ΔG-GFP rVSV (Kerafast, kindly provided by Dr. Michael A. Whitt) at a multiplicity of ~0.02 in serum-free DMEM, and 3 hours later cells were washed twice with PBS, and normal growth medium was added to cells. Cells were incubated at 32°C. Supernatants containing pVSV/ANDV, pVSV/DOBV, or pVSV/VSV-G were collected 24 hours after infection, and supernatants containing pVSV/SNV, pVSV/HTNV, pVSV/SEOV, or pVSV/PUUV was collected 48 hours after infection. Supernatants were clarified by centrifugation and stored at -80°C until use.

Pseudotyped virus neutralization assay

The constructs pVSV/ANDV, pVSV/DOBV, pVSV/SNV, pVSV/HTNV, pVSV/SEOV, and pVSV/PUUV were used in neutralization assays. BHK-21 cells were plated at 5,000 cells/well in a 96-well plate. Antibodies were diluted serially in full growth medium and then incubated with virus for 1 hour at 37°C. Medium containing antibody and virus was added to cells and incubated for 1 hour at 37°C to allow viral attachment. Cells then were washed, and the antibody and virus mixture were removed and replaced with full growth medium. After 24 hours, the medium was removed, the cells were imaged on an CTL ImmunoSpot® S6 Analyzer (CTL), and GFP-positive cells were counted in each well. Percent relative infectivity was calculated by dividing the number of GFP-positive cells in the wells containing antibody, normalized to the average number of GFP-positive cells in wells with only virus.

Receptor blocking assay

A soluble extracellular cadherin repeat 1 (sEC1, GenBank: NM_002587, residues 1 to 172) construct was synthesized and cloned into the pCDNA3.1(+) mammalian cell expression vector by GenScript with a C-terminal GSG linker and decahistidine tag. sEC1 was expressed in ExpiCHO cells and purified through a HisTrap Excel column (Cytiva) using an ÄKTA pure protein purification system (Cytiva), and then labeled with Alexa Fluor 647 (Thermo Fisher). Expi293F cells transfected with a plasmid encoding full-length ANDV M segment, as described previously, were incubated with 10 µg/mL of each mAb for 1 hour at 4°C. A control mAb, DENV 2D22 directed to dengue virus envelope protein, was added as a negative control, and unlabeled sEC1 was added at 50 µg/mL as a positive control. Labeled sEC1 was added directly to the cell suspension and first mAb at a final concentration of 200 ng/mL and incubated for an additional hour at 4°C. Cells then were washed with flow cytometry buffer and stained with 0.5 µg/mL of 4',6-diamidino-2-phenylindole (DAPI). Alexa Fluor 647 and DAPI staining were measured with an iQue Screener Plus flow cytometer (Intellicyt) and quantified using the manufacturer's ForeCyt software. Binding in the presence of antibody was divided by the maximal binding signal of labeled sEC1 alone to determine the % receptor blocking.

Fusion inhibition assay

Cell to cell fusion inhibition assay was adapted from previously published methods (Willensky et al., 2016). Vero cells were plated at 7,500 cells/well in a 96-well plate (Greiner Bio-One). 24 hours later, cells were transfected with 0.2 µL/well of Lipofectamine 3000 and P300 reagent (Thermo Fisher) and 100 ng/well of plasmid pWRG/SN-M (opt) or 75 ng/well of plasmid pWRG/AND-M. 48 hours post transfection, 10 µg/mL of each mAb was incubated for 1 hour on transfected cells at 37°C. Medium containing mAbs was removed and replaced with MES-buffered D-MEM (pH 5.5) and incubated for 5 minutes at 37°C. Cells were washed twice with D-PBS and medium was replaced with normal growth medium (D-MEM, pH 7.4). Cells were incubated for 3 hours at 37°C, and then incubated for an additional hour at 37°C in D-MEM containing 1 µM 5-chloromethylfluorescein diacetate (Cell Tracker CMFDA, Molecular Probes) to stain cytoplasm. Cells were then fixed with 4% (w/v) paraformaldehyde for 20 minutes at room temperature and permeabilized with 0.1% Triton X-100. To stain hantavirus glycoproteins, cells were incubated with a combination of SNV-27, SNV-56 and ANDV-44 (0.5 µg/mL of each in 0.1% BSA) for 1 hour at room temperature, shaking, and then washed twice with PBS-T. Cells were then incubated for 45 minutes (shaking) with Goat anti-human IgG Alexa Fluor 568 (1 µg/mL in 0.1% BSA), washed twice with PBS-T, and then D-PBS containing 0.1 µg/mL of DAPI was added to stain nuclei. Four images per well channel were captured using an Image Xpress (Molecular Devices) fluorescent imager. Fusion index was measured using the MetaXpress software (Molecular Devices) Mi-cronuclei application module. Four images per well were used to count the % of multinucleated cells, and then averaged values were normalized to a control well that was not treated with mAb (representing maximum multinucleated cell formation) to calculate a fusion index (%) for each mAb.

Plaque reduction neutralization assay with authentic SNV or ANDV

For plaque-based neutralization assays, 100 PFU of ANDV strain Chile-9717869 (GenBank: AF291702-04) or SNV strain SN 77734 (GenBank: AF281850-52) from the World Reference Center of Emerging Viruses and Arboviruses were preincubated with various concentrations of mAbs in a 100 µL volume for 1 h at 37°C in triplicate and placed on monolayers of Vero-E6 cells in 96-well plates. After adsorption of the virus for 1 h at 37°C, the virus-antibodies mixture was replaced with 100 µL of 0.9% methylcellulose in minimal essential medium (MEM) containing 10% fetal bovine serum (Quality Biologicals) and 0.1% gentamicin sulfate (Mediatech), followed

by incubation at 37°C for 6 to 7 days for ANDV and 10 to 11 days for SNV. Plates were fixed with 10% buffered formalin (Thermo Fisher) before removal from the biocontainment laboratories. Plaques were visualized by staining monolayers with the mixture of ANDV or SNV monoclonal antibodies. KPL Affinity Purified Peroxidase Labeled Goat Anti-human IgG (SeraCare) were used as secondary antibodies and AEC Substrate Kit (Abcam) as substrate for HRP. Plaques were counted, and neutralization curves were plotted as percentages of reduction of plaques numbers compared to mock-neutralized virus.

Plaque reduction neutralization titer with authentic OWHs

Plaque reduction neutralization tests (PRNT) were performed as previously described with some modifications (Hooper et al., 2001a). Antibodies were diluted in cEMEM and then combined with an equal volume of cEMEM containing 75 PFU of virus and 10% human complement. The antibody-virus mixture was incubated overnight at 2 to 8°C and then adsorbed into 1-week old Vero E6 cell culture monolayers in 6-well plates. After 1 h, a 3 mL agarose overlay was added, and the plates were placed in a 37°C, 5% CO₂ incubator. HTNV- and SEOV-infected monolayers were fixed by adding 2 mL 10% formalin on day 7. PUUV- and DOBV-infected monolayers were fed with 1 mL of additional agarose overlay on day 7 and then fixed with formalin on day 10 or 11. After at least 5 h of fixation, the formalin and agarose overlay were removed and the monolayers were immunostained as previously described (Hooper et al., 2014b). Plaques were stained using mAb 3D7-conjugated to HRP (1:1,000) (Life Sciences) eliminating the need for a secondary antibody. A specific positive control (rabbit serum) was included in each assay. PRNT₅₀ titers were the highest dilutions reducing the number of plaques 50% relative to no-antibody control wells.

Competition-binding assay

Expi293F cells transfected with ANDV or SNV full-length M segment, as described previously, were incubated with 10 µg/mL of the first, unlabeled mAb for 1 hour at 4°C. A second mAb labeled with Alexa Fluor 647 (Thermo Fisher) was added directly to the cell suspension and first mAb at a final concentration of 0.5 µg/mL and incubated for an additional hour at 4°C. Cells then were washed with FACS buffer and stained with 0.1 µg/mL of 4',6-diamidino-2-phenylindole (DAPI). Alexa Fluor 647 and DAPI staining were measured with an iQue Screener Plus flow cytometer (Intelicyt) and quantified using the manufacturer's ForeCyt software. Binding in the presence of the first antibody was normalized to the maximal binding signal of the labeled antibody alone to determine the % competition values.

Expression and purification of recombinant Gc (rGc) protein and ELISA binding assays

A cDNA encoding the ectodomain of Gc from SNV strain SN77734 (GenBank: KF537002.1, residues 661 to 1,103) or ANDV strain AH-1 (GenBank: QNQ18210.1, residues 656 to 1,102) was synthesized with an N-terminal BM40 signal peptide sequence, C-terminal GSG linker, hexahistidine tag and cloned into the pcDNA3.1 (+) vector (Thermo Fisher). The construct then was expressed in ExpiCHO cells and purified through a HisTrap Excel column (Cytiva, formerly GE Healthcare Life Sciences) using an ÄKTA pure protein purification system (Cytiva). 384-well plates were coated with 1 µg/mL of purified rGc protein overnight at 4°C in carbonate buffer (0.03 M NaHCO₃, 0.01 M Na₂CO₃, pH 9.7). Plates were incubated with blocking buffer (5% non-fat dry milk, 2% goat serum in PBS-T) for 1 h at room temperature. Diluted primary antibodies were added to appropriate wells and incubated for 2 h at room temperature, and alkaline-phosphatase-conjugated secondary antibodies (Meridian Life Sciences) were used to detect binding. Phosphatase substrate (Sigma-Aldrich) was added, and plates were developed for 30 min before reading absorbance at 405 nm on a BioTek microplate reader.

Expression of cell-surface-displayed Gn protein and binding assay

A cDNA encoding the full-length Gn coding sequence from SNV strain NMH10 (GenBank accession number: NP_941974, residues 1 to 652) was synthesized and cloned into the pCAGGS vector (Kerafast). The full-length Gn protein coding sequence from ANDV AH-1 (GenBank: QNQ18210.1, residues 1 to 590) was synthesized and cloned into the pcDNA3.1 (+) vector. ExpiCHO cells were transfected transiently with constructs encoding Gn, as described above. Flow cytometry assays were used to measure binding of antibodies to Gn, as described above.

Testing of protective efficacy against ANDV in the Syrian hamster model

Animal challenge studies were conducted in the ABSL-4 facility of the Galveston National Laboratory. The animal protocol for testing of mAbs in hamsters was approved by the Institutional Animal Care and Use Committee (IACUC) of the University of Texas Medical Branch at Galveston (UTMB). 8-week-old female golden Syrian hamsters (*Mesocricetus auratus*) (Envigo) were inoculated with 200 PFU of Andes hantavirus (strain Chile-9717869) by the intramuscular (i.m.) route on day 0. Animals (n = 6 per group) were treated with 5 mg/kg of rSNV-24, rSNV-30, rSNV-53, rANDV-5, rANDV-44 or rDENV 2D22 (a negative control dengue virus antibody) by the intra-peritoneal (i.p.) route on days 3 and 8 after virus inoculation. Animals were weighed and monitored daily over a 26-day period after challenge. Once animals were symptomatic, they were examined twice per day. The disease was scored using the following parameters: breathing abnormalities, hunched posture, ruffed fur, rapid shallow breaths, paucity of movements and weight loss.

Moribund animals were euthanized as specified by the IACUC protocol. Blood was collected on days 8 and 11 of the study, and all animals were euthanized 32 days after infection when terminal bleeding and organ collection (lungs and liver) were performed.

Histopathology

During necropsy, gross lesions were noted and representative lung tissues from the left lobe were collected in 10% formalin (tissues to be fixed were no more than 1 cm³ to ensure formalin penetration). After a 24-hour initial fixation at 4°C, the lung tissues were transferred to fresh 10% formalin for an additional 48-hour fixation, prior to removal from the biocontainment. Formalin-fixed tissues were processed by standard histological procedures by the UTMB Anatomic Pathology Core. About 4-μm-thick sections were cut and stained with hematoxylin and eosin (HE). Sections of lungs were examined for the extent of inflammation, type of inflammatory foci, and changes in alveoli/alveolar septa/airways/blood vessels in parallel with sections from uninfected or control animals. The blinded tissue sections were semiquantitatively scored for pathological lesions using the criteria described (Matute-Bello et al., 2008) (Table S3).

QUANTIFICATION AND STATISTICAL ANALYSIS

Statistical analysis for each experiment is described in [Method details](#) and/or in the figure legends. All statistical analysis was done in Prism v7 (GraphPad) or RStudio v1.3.1073.

Binding and neutralization curves

EC₅₀ values for mAb binding were calculated through a log transformation of antibody concentration using four-parameter dose-response nonlinear regression analysis with a bottom constraint value of zero. IC₅₀ values for mAb-mediated neutralization were calculated through a log transformation of antibody concentration using four-parameter dose-response nonlinear regression analysis with a bottom constraint value of zero and a top constraint value of 100. IC₉₀ values were calculated in the same way as IC₅₀ values, but the F constant was set to ten. EC₅₀, IC₅₀, and IC₉₀ values were generated from 2 to 3 independent experiments and reported as an average value.

Competition-binding analysis

Binding values for mAb-treated samples were normalized to a maximal binding control to determine the residual binding % of each mAb, and values from 3 independent experiments were averaged. Correlation coefficients were determined through Pearson method on RStudio using the “rcorr” function. The mAbs were reordered according to the correlation coefficient using “hclust” method.

Testing of protective efficacy in Syrian hamsters

Studies were done with 6 hamsters per antibody treatment group. Survival curves were created through Kaplan-Meier analysis, and a log-rank (Mantel-Cox) test was used to compare each mAb treatment group to the isotype control (rDENV 2D22) (* p < 0.05, ** p < 0.01, *** p < 0.001).

Update

Cell Reports

Volume 36, Issue 3, 20 July 2021, Page

DOI: <https://doi.org/10.1016/j.celrep.2021.109453>

Correction

Broad and potently neutralizing monoclonal antibodies isolated from human survivors of New World hantavirus infection

Taylor B. Engdahl, Natalia A. Kuzmina, Adam J. Ronk, Chad E. Mire, Matthew A. Hyde, Nurgun Kose, Matthew D. Josley, Rachel E. Sutton, Apoorva Mehta, Rachael M. Wolters, Nicole M. Lloyd, Francisca R. Valdivieso, Thomas G. Ksiazek, Jay W. Hooper, Alexander Bukreyev,* and James E. Crowe, Jr.*

*Correspondence: alexander.bukreyev@utmb.edu (A.B.), james.crowe@vumc.org (J.E.C.)

<https://doi.org/10.1016/j.celrep.2021.109453>

(Cell Reports 35, 109086-1–13.e1–e9; May 4, 2021)

In the originally published version of this article, the incorrect DOI was listed. The original/source data for all figures can be found at <https://doi.org/10.17632/36yhsg4b36.1>. The paper has now been corrected online.

The authors regret this error.

